AIMS Mathematics, 8(11): 25343–25370.
DOI: 10.3934/math.20231293
Received: 12 May 2023
Revised: 24 July 2023
Accepted: 20 August 2023
Published: 01 September 2023

http://www.aimspress.com/journal/Math

Research article

Application of trigonometric B-spline functions for solving Caputo time fractional gas dynamics equation

Rabia Noureen[1], Muhammad Nawaz Naeem[1], Dumitru Baleanu[2,3,4,*], Pshtiwan Othman Mohammed[5,*] and Musawa Yahya Almusawa[6]

[1] Department of Mathematics, Government College University Faisalabad, Faisalabad 38000, Pakistan

[2] Department of Computer Science and Mathematics, Lebanese American University, Beirut 11022801, Lebanon

[3] Institute of Space Sciences, R76900 Magurele-Bucharest, Romania

[4] Department of Medical Research, China Medical University, Taichung 40402, Taiwan

[5] Department of Mathematics, College of Education, University of Sulaimani, Sulaimani 46001, Iraq

[6] Department of Mathematics, Faculty of Science, Jazan University, Jazan 45142, Saudi Arabia

* **Correspondence:** Email: dumitru.baleanu@gmail.com; pshtiwansangawi@gmail.com.

Abstract: In this study, we present a numerical method that utilizes trigonometric cubic B-spline functions to solve the time fractional gas dynamics equation, which is a key component in the study of physical phenomena such as explosions, combustion, detonation and condensation in a moving flow. The Caputo formula is used to define the fractional time derivative, which generalizes the framework for both singular and non-singular kernels. To discretize the unknown function and its derivatives in the spatial direction, we employ trigonometric cubic B-spline functions, while the usual finite difference formulation is used to approximate the Caputo time fractional derivative. A stability analysis of the scheme is provided to ensure that errors do not propagate over time, and a convergence analysis is conducted to measure the accuracy of the solution. To demonstrate the effectiveness of the proposed methodology, we solve various relevant examples and present graphical and tabular results to evaluate the outcomes of the strategy.

Keywords: time fractional gas dynamics equation; trigonometric cubic B-spline functions; finite difference formulation; collocation method; stability; convergence analysis
Mathematics Subject Classification: 33B10, 26A51, 26A48, 39B62, 39A12

1. Introduction

Gas dynamics plays a critical and indispensable role in the design of various apparatus, engines and gas-powered vehicles. It is instrumental in identifying and understanding the forces of pressure, temperature, friction and heat flow that act on a body or duct interacting with gas. By examining the propulsion of gas jets, blast and shock waves, combustion and detonation, gas dynamics enables us to measure the pressure, temperature and other relevant gas characteristics throughout the entire propagation region by its governing laws. The laws of gas dynamics find extensive applications in both exterior and interior ballistics and the study of various phenomena, including explosion, combustion, detonation and condensation in moving gas currents. Moreover, these laws are crucial in the design and analysis of a wide range of engineering devices and systems, such as compressors, turbines, nozzles, diffusers, rocket motors, wind tunnels, ejectors and gas pipelines. To effectively understand and predict the behavior of these phenomena and devices, mathematical modeling plays a central role.

The mathematical model describing the phenomenon of gas dynamics is as follows:

$$ {}^{\mathbf{LC}}\mathfrak{D}_{\wp}^{\mathfrak{B}} s(\varepsilon,\wp) + \mathfrak{C} s(\varepsilon,\wp)\frac{\partial s(\varepsilon,\wp)}{\partial \varepsilon} = \mathfrak{I} s(\varepsilon,\wp)(1 - s(\varepsilon,\wp)) + \mathfrak{x}(\varepsilon,\wp), \quad \dot{a} \le \varepsilon \le \dot{b}, \quad 0 \le \wp \le \mathfrak{T}, \tag{1.1} $$

$$ s(\varepsilon,0) = \varsigma(\varepsilon), \quad \varepsilon \in [\dot{a},\dot{b}], \tag{1.2} $$

$$ s(\dot{a},\wp) = \omega_1(\wp), s(\dot{b},\wp) = \omega_2(\wp), \quad 0 \le \wp \le \mathfrak{T}, \tag{1.3} $$

where $\mathfrak{C}$ and $\mathfrak{I}$ are convection and reaction parameters, correspondingly, $s(\varepsilon,\wp)$ is the state evolution throughout the spatial-temporal domain, $\mathfrak{x}(\varepsilon,\wp)$ is a suitable prescribed function of ε and $\wp$ respectively, $0 < \mathfrak{B} \le 1$ and ${}^{\mathbf{LC}}\mathfrak{D}_{\wp}^{\mathfrak{B}} s(\varepsilon,\wp)$ fractional derivative is expressed in the Caputo perspective as

$$ {}^{\mathbf{LC}}\mathfrak{D}_{\wp}^{\mathfrak{B}} s(\varepsilon,\wp) = \begin{cases} \frac{1}{\Gamma(1-\mathfrak{B})}\int_0^{\wp} \frac{\partial s(\varepsilon,\xi)}{\partial \xi}(\wp-\xi)^{-\mathfrak{B}}, & 0 < \mathfrak{B} < 1, \\ \frac{\partial s(\varepsilon,\wp)}{\partial \wp}, & \mathfrak{B} = 1. \end{cases} \tag{1.4} $$

The exploration of complex fractional partial differential equations has been a highly significant subject of research in the past. So, the analytical and numerical investigation of the time fractional gas dynamics equation (TFGDE) is crucial for understanding and predicting the behavior of gases in complex scenarios [1–4]. Authors in [5] have employed the fractional natural decomposition method to solve TFGDE. Das and Kumar [6] obtained an approximate analytical solution of TFGDE using the differential transform method. Rao and Balaji [7] provided the numerical solution to TFGDE by adopting the Laplace Adomian decomposition method coupled with fractional complex transform. Saad et al. [8] stimulated efficient technique, namely the optimal q-homotopy method for space and TFGDE. Iqbal et al. [9] presented an iterative transformation technique and homotopy perturbation method combined with Elzaki transformation to obtain the analytical solutions of TFGDE. With the advent of computers, splines have gained significant prominence in various fields of mathematics and engineering. The authors in [10–12] have made significant contributions to the analysis of numerical solutions of differential equations using various spline methods. In their work, they have extensively explored and compared the effectiveness of three different spline methods: the spline method, the modified spline method and the orthogonal spline method. Esen and Tasbozan [13, 14] proposed the cubic B-spline collocation method and the quadratic B-spline Galerkin method to investigate the approximate solution of TFGDE.

Trigonometric B-splines have been proven to be highly effective in addressing surface approximation problems in geometric modeling, as highlighted by Wang and Chen in their research [15]. These special functions are well-known for their shape-preserving interpolation properties and geometric characteristics, such as C^2 continuity, non-negativity and partition of unity. Due to these desirable properties, trigonometric B-splines find extensive use in image processing and computer graphics, where they are employed for tasks like image interpolation, smoothing and compression. The wide applicability of trigonometric B-splines has led to the proposal of various forms of these functions as alternatives to the more common polynomial B-splines. Researchers, such as Nazir and Abbas [16], Ay and Dag [17], Yaseen and Abbas [18–20] and Abbas and Majid [21], have contributed to the development and exploration of different formulations of trigonometric B-splines.

In the current manuscript, our primary objective is to explore the practical applications of trigonometric cubic B-spline functions in combination with the collocation method. We aim to demonstrate the utility of these spline functions in tackling the TFGDE and to present a systematic solution algorithm for effectively solving this equation. We have rigorously derived theoretical results for the stability and convergence analysis of the proposed algorithm. To assess the accuracy performance of the proposed method, we have conducted extensive investigations using various test problems relevant to gas dynamics.

The manuscript is structured as follows: In Section 2, the authors introduce a numerical approach based on trigonometric B-splines. Sections 3 and 4 address the stability analysis and theoretical convergence of the analyzed system, respectively. The key findings for the investigated interacting mechanism are derived in Section 5 and we conclude with several comments on the acquired outcomes in Section 6.

2. Description of numerical approach

Consider the subdivision of temporal domain $[0, \mathfrak{T}]$ into $\mathbb{M}$ equal sub-intervals $[\wp_{\mathfrak{m}}, \wp_{\mathfrak{m}+1}]$ of the length $\Delta\wp = \frac{\mathfrak{T}}{\mathbb{M}}$ using the knots $0 = \wp_0 < \wp_1 < ... < \wp_{\mathbb{M}} = \mathfrak{T}$, where $\wp_m = m\Delta\wp, \quad m = 0, 1, ..., \mathbb{M}$. The time fractional derivative expressed in Eq (1.4) can be approximated at $\wp = \wp_{\mathfrak{m}+1}$ with the help of $L1$ formula described as [18]:

$$ {}^{\mathbf{LC}}\mathfrak{D}_{\wp}^{\mathfrak{B}} s(\varepsilon, \wp_{m+1}) = \frac{1}{\Gamma(2-\mathfrak{B})} \sum_{\varphi=0}^{\mathfrak{m}} \mathfrak{r}_{\varphi} \frac{s(\varepsilon, \wp_{\mathfrak{m}-\varphi+1}) - s(\varepsilon, \wp_{\mathfrak{m}-\varphi})}{(\Delta\wp)^{\mathfrak{B}}} + \mathbb{E}^{\mathfrak{m}+1}, \tag{2.1} $$

where $\mathfrak{r}_{\varphi} = (\varphi+1)^{1-\mathfrak{B}} - \varphi^{1-\mathfrak{B}}$ and the truncation error $\mathbb{E}^{\mathfrak{m}+1}$ is bounded.

$$ |\mathbb{E}^{\mathfrak{m}+1}| \leq \mathrm{Re}_s (\Delta\wp)^{2-\mathfrak{B}}, \tag{2.2} $$

where Re_s is constant.

The co-efficients $\mathfrak{r}_{\varphi}$ fulfill the following regulations:

$$ \begin{cases} \mathfrak{r}_0 = 1, \\ \mathfrak{r}_0 > \mathfrak{r}_1 > \mathfrak{r}_2 > ... > \mathfrak{r}_{\varphi}, \quad \mathfrak{r}_{\varphi} \to 0 \ \text{ as } \ \varphi \to \infty, \\ \mathfrak{r}_{\varphi} > 0, \ \text{ for } \ \varphi = 0, 1, 2, ...\mathfrak{m}, \\ \sum_{\varphi=0}^{\mathfrak{m}} (\mathfrak{r}_{\varphi} - \mathfrak{r}_{\varphi+1}) + \mathfrak{r}_{\varphi+1} = (1 - \mathfrak{r}_1) + \sum_{\varphi=1}^{\mathfrak{m}-1} (\mathfrak{r}_{\varphi} - \mathfrak{r}_{\varphi+1}) + \mathfrak{r}_{\varphi} = 1. \end{cases} \tag{2.3} $$

Employing Eq (2.1) combined with a θ-weighted scheme, Eq (1.1) transforms into the following form as

$$\begin{aligned}&\mathrm{Im}\sum_{\varphi=0}^{\mathfrak{m}}\mathfrak{r}_{\varphi}[s^{\mathfrak{m}-\varphi+1}-s^{\mathfrak{m}-\varphi}]+\theta[\mathfrak{C}(ss_{\varepsilon})^{\mathfrak{m}+1}-\mathfrak{I}(s-s^{2})^{\mathfrak{m}+1}]+(1-\theta)[\mathfrak{C}(ss_{\varepsilon})^{\mathfrak{m}}-\mathfrak{I}(s-s^{2})^{\mathfrak{m}}]\\&=\mathfrak{X}^{\mathfrak{m}+1},\quad \mathfrak{m}=0,1,2,...,\mathbb{M}-1,\end{aligned}\tag{2.4}$$

where $\mathrm{Im}=\frac{1}{(\Delta\wp)^{\mathfrak{B}}\Gamma(2-\mathfrak{B})}$, $s^{\mathfrak{m}}=s(\varepsilon,\wp_{\mathfrak{m}})$ and $\mathfrak{X}^{\mathfrak{m}+1}=\theta\mathfrak{x}^{\mathfrak{m}+1}+(1-\theta)\mathfrak{x}^{\mathfrak{m}}$. Rubin and Graves [22] advertised the following formula to linearize the nonlinear terms:

$$\begin{cases}(ss_{\varepsilon})^{\mathfrak{m}+1}=s^{\mathfrak{m}+1}s_{\varepsilon}^{\mathfrak{m}}+s^{\mathfrak{m}}s_{\varepsilon}^{\mathfrak{m}+1}-s^{\mathfrak{m}}s_{\varepsilon}^{\mathfrak{m}},\\(s^{2})^{\mathfrak{m}+1}=2s^{\mathfrak{m}+1}s^{\mathfrak{m}}-s^{\mathfrak{m}}s^{\mathfrak{m}}.\end{cases}\tag{2.5}$$

Utilizing Eq (2.5) in Eq (2.4) as

$$\Phi^{\mathfrak{m}}s^{\mathfrak{m}+1}+\Psi^{\mathfrak{m}}s_{\varepsilon}^{\mathfrak{m}+1}=\Upsilon^{\mathfrak{m}}s^{\mathfrak{m}}-\mathrm{Im}\sum_{\varphi=1}^{\mathfrak{m}}\mathfrak{r}_{\varphi}[s^{\mathfrak{m}-\varphi+1}-s^{\mathfrak{m}-\varphi}]+\mathfrak{X}^{\mathfrak{m}+1},\tag{2.6}$$

where

$$\begin{aligned}\Phi^{\mathfrak{m}}&=\mathrm{Im}+\mathfrak{C}\theta s_{\varepsilon}^{\mathfrak{m}}-\theta\mathfrak{I}+2\theta\mathfrak{I}s^{\mathfrak{m}},\qquad \Psi^{\mathfrak{m}}=\theta\mathfrak{C}s^{\mathfrak{m}},\\\Upsilon^{\mathfrak{m}}&=\mathrm{Im}+\theta\mathfrak{C}s_{\varepsilon}^{\mathfrak{m}}+\theta\mathfrak{I}s^{\mathfrak{m}}-(1-\theta)\Big[\mathfrak{C}s_{\varepsilon}^{\mathfrak{m}}-\mathfrak{I}+\mathfrak{I}s^{\mathfrak{m}}\Big].\end{aligned}$$

Let us assume the spatial domain $[\dot{a},\dot{b}]$ is uniformly partitioned into $\mathbb{L}$ subdomains of step distance $\mathfrak{h}$ by inserting the knots $\varepsilon_{\mathfrak{l}}$ such that $\dot{a}=\varepsilon_0<\varepsilon_1<...<\varepsilon_{\mathbb{L}}=\dot{b}$ where $\mathfrak{h}=\varepsilon_{\mathfrak{l}+1}-\varepsilon_{\mathfrak{l}},\ \ \mathfrak{l}=0,1,2,...\mathbb{L}$. Our scheme for solving Eq (1.1) demands approximate solution $\mathbb{S}(\varepsilon,\wp)$ to the exact solution $s(\varepsilon,\wp)$ in the ensuing form [23, 24]:

$$\mathbb{S}(\varepsilon,\wp)=\sum_{\mathfrak{l}=-1}^{\mathbb{L}+1}\aleph_{\mathfrak{l}}^{\mathfrak{m}}(\wp)\mathbb{T}_{\mathfrak{l}}(\varepsilon),\tag{2.7}$$

where time-dependent unknowns $\aleph_{\mathfrak{l}}^{\mathfrak{m}}(\wp)$ are to be determined from the boundary and trigonometric cubic B-spline collocation conditions and $\mathbb{T}_{\mathfrak{l}}(\varepsilon)$ are twice continuously differentiable trigonometric cubic B-spline functions, described as follows [19]:

$$\mathbb{T}_{\mathfrak{l}}(\varepsilon)=\frac{1}{\mathbb{W}}\begin{cases}\eta^{3}(\varepsilon_{\mathfrak{l}-2}), & \varepsilon\in[\varepsilon_{\mathfrak{l}-2},\varepsilon_{\mathfrak{l}-1}],\\\eta(\varepsilon_{\mathfrak{l}-2})\Big(\eta(\varepsilon_{\mathfrak{l}-2})\varrho(\varepsilon_{\mathfrak{l}})+\varrho(\varepsilon_{\mathfrak{l}+1})\eta(\varepsilon_{\mathfrak{l}-1})\Big)+\varrho(\varepsilon_{\mathfrak{l}+2})\eta^{2}(\varepsilon_{\mathfrak{l}-1}), & \varepsilon\in[\varepsilon_{\mathfrak{l}-1},\varepsilon_{\mathfrak{l}}],\\\varrho(\varepsilon_{\mathfrak{l}+1})\Big(\eta(\varepsilon_{\mathfrak{l}-2})\varrho(\varepsilon_{\mathfrak{l}+1})+\varrho(\varepsilon_{\mathfrak{l}+2})\eta(\varepsilon_{\mathfrak{l}-1})\Big)+\eta(\varepsilon_{\mathfrak{l}})\varrho^{2}(\varepsilon_{\mathfrak{l}+2}), & \varepsilon\in[\varepsilon_{\mathfrak{l}},\varepsilon_{\mathfrak{l}+1}],\\\varrho^{3}(\varepsilon_{\mathfrak{l}+2}), & \varepsilon\in[\varepsilon_{\mathfrak{l}+1},\varepsilon_{\mathfrak{l}+2}],\end{cases}\tag{2.8}$$

where

$$\eta(\varepsilon_{\mathfrak{l}})=\sin\Big(\frac{\varepsilon-\varepsilon_{\mathfrak{l}}}{2}\Big),\quad \varrho(\varepsilon_{\mathfrak{l}})=\sin\Big(\frac{\varepsilon_{\mathfrak{l}}-\varepsilon}{2}\Big),\quad \mathbb{W}=\sin\Big(\frac{\mathfrak{h}}{2}\Big)\sin\Big(\mathfrak{h}\Big)\sin\Big(\frac{3\mathfrak{h}}{2}\Big).$$

The support of the B-spline functions $\mathbb{T}_{\mathfrak{l}}(\varepsilon)$ is assumed to be $[\varepsilon_{\mathfrak{l}-2},\varepsilon_{\mathfrak{l}+2}]$. Notice that each $\mathbb{T}_{\mathfrak{l}}(\varepsilon)$ is piecewise cubic and nonzero over four consecutive sub-domains and die out otherwise. Consequently, each sub-domain $[\varepsilon_{\mathfrak{l}},\varepsilon_{\mathfrak{l}+1}]$ contains three segments of $\mathbb{T}_{\mathfrak{l}}(\varepsilon)$.

Equation (2.6) in terms of approximate solution (2.7) can be written as

$$\Phi^{\mathfrak{m}}\mathbb{S}^{\mathfrak{m}+1} + \Psi^{\mathfrak{m}}\mathbb{S}_{\varepsilon}^{\mathfrak{m}+1} = \Upsilon^{\mathfrak{m}}\mathbb{S}^{\mathfrak{m}} - \mathrm{Im}\sum_{\varphi=1}^{\mathfrak{m}} \mathfrak{r}_{\varphi}[\mathbb{S}^{\mathfrak{m}-\varphi+1} - \mathbb{S}^{\mathfrak{m}-\varphi}] + \mathfrak{X}^{\mathfrak{m}+1}. \tag{2.9}$$

Discretizing the above Eq (2.9) along the spatial grid gives

$$\Phi^{\mathfrak{m}}\mathbb{S}_{\mathfrak{l}}^{\mathfrak{m}+1} + \Psi^{\mathfrak{m}}(\mathbb{S}_{\varepsilon})_{\mathfrak{l}}^{\mathfrak{m}+1} = \Upsilon^{\mathfrak{m}}\mathbb{S}_{\mathfrak{l}}^{\mathfrak{m}} - \mathrm{Im}\sum_{\varphi=1}^{\mathfrak{m}} \mathfrak{r}_{\varphi}[\mathbb{S}_{\mathfrak{l}}^{\mathfrak{m}-\varphi+1} - \mathbb{S}_{\mathfrak{l}}^{\mathfrak{m}-\varphi}] + \mathfrak{X}^{\mathfrak{m}+1}. \tag{2.10}$$

Using Eqs (2.7) and (2.8), the expression of $\mathbb{S}(\varepsilon, \wp)$ and its necessary spatial derivatives at the nodal points are determined in terms of the parameters $\aleph_{\mathfrak{l}}$ as follows:

$$\begin{aligned}
\mathbb{S}(\varepsilon_{\mathfrak{l}}, \wp^{\mathfrak{m}}) &= \chi_1\aleph_{\mathfrak{l}-1}^{\mathfrak{m}}(\wp) + \chi_2\aleph_{\mathfrak{l}}^{\mathfrak{m}}(\wp) + \chi_1\aleph_{\mathfrak{l}+1}^{\mathfrak{m}}(\wp),\\
\mathbb{S}_{\varepsilon}(\varepsilon_{\mathfrak{l}}, \wp^{\mathfrak{m}}) &= -\chi_3\aleph_{\mathfrak{l}-1}^{\mathfrak{m}}(\wp) + \chi_3\aleph_{\mathfrak{l}+1}^{\mathfrak{m}}(\wp),\\
\mathbb{S}_{\varepsilon\varepsilon}(\varepsilon_{\mathfrak{l}}, \wp^{\mathfrak{m}}) &= \chi_4\aleph_{\mathfrak{l}-1}^{\mathfrak{m}}(\wp) + \chi_5\aleph_{\mathfrak{l}}^{\mathfrak{m}}(\wp) + \chi_4\aleph_{\mathfrak{l}+1}^{\mathfrak{m}}(\wp),
\end{aligned} \tag{2.11}$$

where

$$\chi_1 = \csc\left(\mathfrak{h}\right)\csc\left(\frac{3\mathfrak{h}}{2}\right)\sin^2\left(\frac{\mathfrak{h}}{2}\right),\ \chi_2 = \frac{2}{1+2\cos\mathfrak{h}},\ \chi_3 = \frac{3}{4}\csc\left(\frac{3\mathfrak{h}}{2}\right),$$

$$\chi_4 = \frac{3+9\cos\mathfrak{h}}{4\cos\left(\frac{\mathfrak{h}}{2}\right) - 4\cos\left(\frac{5\mathfrak{h}}{2}\right)},\ \chi_5 = -\frac{3\cot^2\left(\frac{\mathfrak{h}}{2}\right)}{2+4\cos(\mathfrak{h})}.$$

Substituting Eq (2.11) into Eq (2.10) gives

$$\begin{aligned}
&\left(\chi_1\Phi_{\mathfrak{l}}^{\mathfrak{m}} - \chi_3\Psi_{\mathfrak{l}}^{\mathfrak{m}}\right)\aleph_{\mathfrak{l}-1}^{\mathfrak{m}+1} + \chi_2\Phi_{\mathfrak{l}}^{\mathfrak{m}}\aleph_{\mathfrak{l}}^{\mathfrak{m}+1} + \left(\chi_1\Phi_{\mathfrak{l}}^{\mathfrak{m}} + \chi_3\Psi_{\mathfrak{l}}^{\mathfrak{m}}\right)\aleph_{\mathfrak{l}+1}^{\mathfrak{m}+1}\\
=&\chi_1\Upsilon_{\mathfrak{l}}^{\mathfrak{m}}\aleph_{\mathfrak{l}-1}^{\mathfrak{m}} + \chi_2\Upsilon_{\mathfrak{l}}^{\mathfrak{m}}\aleph_{\mathfrak{l}}^{\mathfrak{m}} + \chi_1\Upsilon_{\mathfrak{l}}^{\mathfrak{m}}\aleph_{\mathfrak{l}+1}^{\mathfrak{m}} - \mathrm{Im}\sum_{\varphi=1}^{\mathfrak{m}} \mathfrak{r}_{\varphi}\Big[\chi_1(\aleph_{\mathfrak{l}-1}^{\mathfrak{m}-\varphi+1} - \aleph_{\mathfrak{l}-1}^{\mathfrak{m}-\varphi}) + \chi_2(\aleph_{\mathfrak{l}}^{\mathfrak{m}-\varphi+1} - \aleph_{\mathfrak{l}}^{\mathfrak{m}-\varphi})\\
&+ \chi_1(\aleph_{\mathfrak{l}+1}^{\mathfrak{m}-\varphi+1} - \aleph_{\mathfrak{l}+1}^{\mathfrak{m}-\varphi})\Big] + \mathfrak{X}^{\mathfrak{m}+1}, \quad 0 \le \mathfrak{m} \le \mathbb{M},\ 0 \le \mathfrak{l} \le \mathbb{L}.
\end{aligned} \tag{2.12}$$

Framework (2.12) is a system of $(\mathbb{L}+1)$ equations in $(\mathbb{L}+3)$ unknown parameters. Boundary conditions are used to procure two more equations. Consequently, we acquire a consistent diagonal system, which can be solved using any suitable algorithm based on Gaussian elimination.

2.1. Initial vector

The initial vector $\aleph^0 = [\aleph_{-1}^0, \aleph_0^0, ..., \aleph_{\mathbb{L}+1}^0]^T$ is needed to start the iterative process, which can be captured from the initial condition and its first derivatives at the endpoints as follows:

$$\begin{aligned}
\mathbb{S}_0' &= \varsigma'(\varepsilon_0),\\
\mathbb{S}_{\mathbb{L}}^0 &= \varsigma(\varepsilon_{\mathfrak{l}}),\ \ \mathfrak{l} = 0, 1, 2, ..., \mathbb{L},
\end{aligned} \tag{2.13}$$

$$\mathbb{S}'_{\mathbb{L}} = \varsigma'(\varepsilon_{\mathbb{L}}).$$

This yields the following $(\mathbb{L}+3)\times(\mathbb{L}+3)$ matrix system:

$$\begin{bmatrix} -\chi_3 & 0 & \chi_3 & 0 & \cdots & 0 & 0 & 0 \\ \chi_1 & \chi_2 & \chi_1 & 0 & \cdots & 0 & 0 & 0 \\ \vdots & \vdots & \vdots & \vdots & \ddots & \vdots & \vdots & \vdots \\ 0 & 0 & 0 & 0 & \cdots & \chi_1 & \chi_2 & \chi_1 \\ 0 & 0 & 0 & 0 & \cdots & -\chi_3 & 0 & \chi_3 \end{bmatrix} \begin{bmatrix} \aleph^0_{-1} \\ \aleph^0_0 \\ \vdots \\ \aleph^0_{\mathbb{L}} \\ \aleph^0_{\mathbb{L}+1} \end{bmatrix} = \begin{bmatrix} (\varsigma_\varepsilon)^0_0 \\ \varsigma^0_0 \\ \vdots \\ \varsigma^0_{\mathbb{L}} \\ (\varsigma_\varepsilon)^0_{\mathbb{L}} \end{bmatrix}.$$

The above system is easily solvable for $\aleph^0$ by means of a suitable numerical algorithm. All the numerical computations are performed in Mathematica 12.

3. Stability

Here, we examine scheme (2.12) for the stability analysis. According to Duhamels' principle, stability analysis for an inhomogeneous problem is typically assumed to be an immediate outcome of the stability analysis for the corresponding homogeneous case. So it is sufficient to provide the stability analysis for the homogenous case $\mathfrak{x}(\varepsilon,\wp)=0$ of Eq (1.1) as follows:

$${}^{\mathbf{LC}}\mathfrak{D}^{\mathfrak{B}}_{\wp} s(\varepsilon,\wp) + \mathfrak{C} s(\varepsilon,\wp)\frac{\partial s(\varepsilon,\wp)}{\partial \varepsilon} = \mathfrak{I} s(\varepsilon,\wp)(1-s(\varepsilon,\wp)), \;\; \dot{a} \le \varepsilon \le \dot{b}, \;\; 0 \le \wp \le \mathfrak{T}. \tag{3.1}$$

We first consider the term s a local constant $\varnothing$, as is done in Von Neumann method. Substituting the approximate solution $\mathbb{S}$, their derivatives at the knots with $\theta = 1$, into Eq (3.1) yields the equation given by

$$\begin{aligned} &\Big(\mathrm{Im}\,\chi_1 - \mathfrak{C}\varnothing\chi_3 - \mathfrak{I}(1-\varnothing)\chi_1\Big)\aleph^{\mathfrak{m}+1}_{\mathfrak{l}-1} + \Big(\mathrm{Im}\,\chi_2 - \mathfrak{I}(1-\varnothing)\chi_2\Big)\aleph^{\mathfrak{m}+1}_{\mathfrak{l}} \\ &+ \Big(\mathrm{Im}\,\chi_1 + \mathfrak{C}\varnothing\chi_3 - \mathfrak{I}(1-\varnothing)\chi_1\Big)\aleph^{\mathfrak{m}+1}_{\mathfrak{l}+1} \\ &= \mathrm{Im}\,\chi_1\aleph^{\mathfrak{m}}_{\mathfrak{l}-1} + \mathrm{Im}\,\chi_2\aleph^{\mathfrak{m}}_{\mathfrak{l}} + \mathrm{Im}\,\chi_1\aleph^{\mathfrak{m}}_{\mathfrak{l}+1} - \mathrm{Im}\sum_{\varphi=1}^{\mathfrak{m}} \mathfrak{r}_\varphi\Big[\chi_1(\aleph^{\mathfrak{m}-\varphi+1}_{\mathfrak{l}-1} - \aleph^{\mathfrak{m}-\varphi}_{\mathfrak{l}-1}) \\ &+ \chi_2(\aleph^{\mathfrak{m}-\varphi+1}_{\mathfrak{l}} - \aleph^{\mathfrak{m}-\varphi}_{\mathfrak{l}}) + \chi_1(\aleph^{\mathfrak{m}-\varphi+1}_{\mathfrak{l}+1} - \aleph^{\mathfrak{m}-\varphi}_{\mathfrak{l}+1})\Big], \;\; 0 \le \mathfrak{m} \le \mathbb{M}, \; 0 \le \mathfrak{l} \le \mathbb{L}. \end{aligned} \tag{3.2}$$

Let $\propto$ and $\breve{\propto}$ be the growth factor and its approximation, respectively, of a Fourier mode. Defining $\Lambda^{\mathfrak{m}}_{\mathfrak{l}} = \propto - \breve{\propto}$, which on substituting in Eq (3.2) gives

$$\begin{aligned} &\Big(\mathrm{Im}\,\chi_1 - \mathfrak{C}\varnothing\chi_3 - \mathfrak{I}(1-\varnothing)\chi_1\Big)\Lambda^{\mathfrak{m}+1}_{\mathfrak{l}-1} + \Big(\mathrm{Im}\,\chi_2 - \mathfrak{I}(1-\varnothing)\chi_2\Big)\Lambda^{\mathfrak{m}+1}_{\mathfrak{l}} \\ &+ \Big(\mathrm{Im}\,\chi_1 + \mathfrak{C}\varnothing\chi_3 - \mathfrak{I}(1-\varnothing)\chi_1\Big)\Lambda^{\mathfrak{m}+1}_{\mathfrak{l}+1} \\ &= \mathrm{Im}\,\chi_1\Lambda^{\mathfrak{m}}_{\mathfrak{l}-1} + \mathrm{Im}\,\chi_2\Lambda^{\mathfrak{m}}_{\mathfrak{l}} + \mathrm{Im}\,\chi_1\Lambda^{\mathfrak{m}}_{\mathfrak{l}+1} - \mathrm{Im}\sum_{\varphi=1}^{\mathfrak{m}} \mathfrak{r}_\varphi\Big[\chi_1(\Lambda^{\mathfrak{m}-\varphi+1}_{\mathfrak{l}-1} - \Lambda^{\mathfrak{m}-\varphi}_{\mathfrak{l}-1}) \\ &+ \chi_2(\Lambda^{\mathfrak{m}-\varphi+1}_{\mathfrak{l}} - \Lambda^{\mathfrak{m}-\varphi}_{\mathfrak{l}}) + \chi_1(\Lambda^{\mathfrak{m}-\varphi+1}_{\mathfrak{l}+1} - \Lambda^{\mathfrak{m}-\varphi}_{\mathfrak{l}+1})\Big]. \end{aligned} \tag{3.3}$$

The above error equation fulfills the initial and boundary conditions:

$$\Lambda_{\mathfrak{l}}^{0} = \varsigma(\varepsilon_{\mathfrak{l}}), \quad \mathfrak{l} = 1, 2, ..., \mathbb{L}, \tag{3.4}$$

$$\Lambda_{0}^{\mathfrak{m}} = \omega_1(\wp^{\mathfrak{m}}), \ \ \Lambda_{\mathbb{L}}^{\mathfrak{m}} = \omega_2(\wp^{\mathfrak{m}}), \quad \mathfrak{m} = 0, 1, ..., \mathbb{M}. \tag{3.5}$$

Define the grid function

$$\Lambda^{\mathfrak{m}} = \begin{cases} \Lambda_{\mathfrak{l}}^{\mathfrak{m}}, \ \ \varepsilon_{\mathfrak{l}} - \frac{\mathfrak{h}}{2} < \varepsilon \leq \varepsilon_{\mathfrak{l}} + \frac{\mathfrak{h}}{2}, \ \ \mathfrak{l} = 1 : 1 : \mathbb{L} - 1, \\ 0, \quad \dot{a} \leq \varepsilon \leq \dot{a} + \frac{\mathfrak{h}}{2} \ \ \text{or} \ \ \dot{b} - \frac{\mathfrak{h}}{2} \leq \varepsilon \leq \dot{b}. \end{cases} \tag{3.6}$$

Notice that the Fourier expansion of $\Lambda^{\mathfrak{m}}(\varepsilon)$ is

$$\Lambda^{\mathfrak{m}}(\varepsilon) = \sum_{\mathfrak{g}=-\infty}^{\infty} \Omega^{\mathfrak{m}}(\mathfrak{g}) e^{\frac{2\pi\iota\varepsilon\mathfrak{g}}{\dot{b}-\dot{a}}}, \ \ \mathfrak{m} = 1, 2, ..., \mathbb{M}, \tag{3.7}$$

where

$$\Omega^{\mathfrak{m}}(\mathfrak{g}) = \frac{1}{\dot{b} - \dot{a}} \int_{\dot{a}}^{\dot{b}} \Lambda^{\mathfrak{m}}(\varepsilon) e^{-\frac{2\pi\iota\mathfrak{g}\varepsilon}{\dot{b}-\dot{a}}} d\varepsilon. \tag{3.8}$$

Let

$$\Lambda^{\mathfrak{m}} = [\Lambda_1^{\mathfrak{m}}, \Lambda_2^{\mathfrak{m}}, ..., \Lambda_{\mathbb{L}-1}^{\mathfrak{m}}]^T,$$

and introduce the norm

$$||\Lambda^{\mathfrak{m}}||_2 = \Big(\sum_{\mathfrak{l}=1}^{\mathbb{L}-1} \mathfrak{h} |\Lambda_{\mathfrak{l}}^{\mathfrak{m}}|^2 \Big)^{\frac{1}{2}} = \Big[\int_{\dot{a}}^{\dot{b}} |\Lambda^{\mathfrak{m}}|^2 d\varepsilon \Big]^{\frac{1}{2}}.$$

By Parseval equality, we have

$$\int_{\dot{a}}^{\dot{b}} |\Lambda^{\mathfrak{m}}|^2 d\varepsilon = \sum_{\mathfrak{g}=-\infty}^{\infty} |\Omega^{\mathfrak{m}}(\mathfrak{g})|^2,$$

which implies that

$$||\Lambda^{\mathfrak{m}}||_2^2 = \sum_{\mathfrak{g}=-\infty}^{\infty} |\Omega^{\mathfrak{m}}(\mathfrak{g})|^2. \tag{3.9}$$

Suppose that Eqs (3.3)–(3.5) have solutions of the form $\Lambda_{\mathfrak{l}}^{\mathfrak{m}} = \zeta^{\mathfrak{m}} e^{\iota\gamma\mathfrak{l}\varepsilon}$, where $\iota = \sqrt{-1}$ and $\gamma \in [-\pi, \pi]$. Substituting this expression in Eq (3.3) and dividing by $e^{\iota\gamma\mathfrak{l}\varepsilon}$, we obtain

$$\begin{aligned} &\Big[\Big(\mathrm{Im}\chi_1 - \Im(1 - \varnothing)\chi_1 \Big) \Big(e^{\iota\gamma\varepsilon} + e^{-\iota\gamma\varepsilon} \Big) + \mathfrak{C}\varnothing\chi_3 \Big(e^{\iota\gamma\varepsilon} - e^{-\iota\gamma\varepsilon} \Big) + \mathrm{Im}\chi_2 - \Im(1 - \varnothing)\chi_2 \Big] \zeta^{\mathfrak{m}+1} \\ =&\zeta^{\mathfrak{m}} \Big[\mathrm{Im}\chi_1 \Big(e^{\iota\gamma\varepsilon} + e^{-\iota\gamma\varepsilon} \Big) + \mathrm{Im}\chi_2 \Big] - \sum_{\varphi=1}^{\mathfrak{m}} \mathfrak{r}_{\varphi} \Big[\Big(\zeta^{\mathfrak{m}-\varphi+1} - \zeta^{\mathfrak{m}-\varphi} \Big) \Big(\mathrm{Im}\chi_1 (e^{\iota\gamma\varepsilon} + e^{-\iota\gamma\varepsilon}) + \mathrm{Im}\chi_2 \Big) \Big]. \end{aligned} \tag{3.10}$$

Using the relations

$$e^{\iota\gamma\varepsilon} + e^{-\iota\gamma\varepsilon} = 2\cos(\gamma\varepsilon),$$
$$e^{\iota\gamma\varepsilon} - e^{-\iota\gamma\varepsilon} = 2\iota\sin(\gamma\varepsilon),$$

and grouping the similar terms, we obtain the following relation:

$$\begin{aligned}&\Big[\Big(\operatorname{Im}\chi_1-\Im(1-\varnothing)\chi_1\Big)(2\cos(\gamma\varepsilon))+\complement\varnothing\chi_3(2\imath\sin(\gamma\varepsilon))+\operatorname{Im}\chi_2-\Im(1-\varnothing)\chi_2\Big]\zeta^{\mathfrak{m}+1}\\&=\zeta^{\mathfrak{m}}\Big[\operatorname{Im}\chi_1(2\cos(\gamma\varepsilon))+\operatorname{Im}\chi_2\Big]-\sum_{\varphi=1}^{\mathfrak{m}}\mathfrak{r}_\varphi\Big[\Big(\zeta^{\mathfrak{m}-\varphi+1}-\zeta^{\mathfrak{m}-\varphi}\Big)\Big(\operatorname{Im}\chi_1(2\cos(\gamma\varepsilon))+\operatorname{Im}\chi_2\Big)\Big].\end{aligned}\tag{3.11}$$

Without any loss of generality, we can suppose that $\gamma = 0$. Then, the last expression reduces to

$$\zeta^{\mathfrak{m}+1}=\frac{1}{\vartheta}\zeta^{\mathfrak{m}}-\frac{1}{\vartheta}\sum_{\varphi=1}^{\mathfrak{m}}\mathfrak{r}_\varphi(\zeta^{\mathfrak{m}-\varphi+1}-\zeta^{\mathfrak{m}-\varphi}),\tag{3.12}$$

where $\vartheta = 1+\frac{2\Im(1-\varnothing)\chi_1+\Im(1-\varnothing)\chi_2}{2\operatorname{Im}\chi_1+\operatorname{Im}\chi_2}$.

Now we have to show that

$$|\zeta^{\mathfrak{m}}|\le|\zeta^0|,\quad \mathfrak{m}=1,2,...,\mathbb{M}.\tag{3.13}$$

With the help of mathematical induction, we have to conclude this result. For $\mathfrak{m} = 0$, we have from Eq (3.12) that

$$|\zeta^1|=\frac{1}{\vartheta}|\zeta^0|\le|\zeta^0|,\qquad\because\quad\frac{1}{\vartheta}<1.\tag{3.14}$$

Assume that $|\zeta^{\mathfrak{m}}|\le|\zeta^0|$ for $\mathfrak{m}=0,1,2,...,\mathbb{M}-1$. We have to prove it for $\mathfrak{m}=k+1$. Now consider

$$\begin{aligned}|\zeta^{k+1}|&=|\frac{1}{\vartheta}\zeta^k-\frac{1}{\vartheta}\sum_{\varphi=1}^{k}\mathfrak{r}_\varphi(\zeta^{k-\varphi+1}-\zeta^{k-\varphi})|\\&\le|\frac{1}{\vartheta}\zeta^k|+|\frac{1}{\vartheta}\sum_{\varphi=1}^{k}\mathfrak{r}_\varphi(\zeta^{k-\varphi+1}-\zeta^{k-\varphi})|\\&\le|\frac{1}{\vartheta}\zeta^k|+\frac{1}{\vartheta}\sum_{\varphi=1}^{k}\mathfrak{r}_\varphi|(\zeta^{k-\varphi+1}-\zeta^{k-\varphi})|\\&\le\frac{1}{\vartheta}|\zeta^k|+\frac{1}{\vartheta}\sum_{\varphi=1}^{k}\Big[|\zeta^{k-\varphi+1}|+|\zeta^{k-\varphi}|\Big],\qquad\because\quad 0<\mathfrak{r}_\varphi\le1,\\&\le\frac{1}{\vartheta}|\zeta^0|+\frac{1}{\vartheta}\sum_{\varphi=1}^{k}\Big[|\zeta^0|+|\zeta^0|\Big]\\&=\frac{1}{\vartheta}|\zeta^0|+\frac{2k}{\vartheta}|\zeta^0|\\&=\frac{1+2k}{\vartheta}|\zeta^0|.\end{aligned}$$

Hence,

$$|\zeta^{k+1}|\le|\zeta^0|,\quad\text{if}\quad\frac{1+2k}{\vartheta}<1.\tag{3.15}$$

From Eqs (3.9) and (3.15), it follows that

$$\|\Lambda_{\mathfrak{l}}^{\mathfrak{m}}\|_2\le\|\Lambda_{\mathfrak{l}}^0\|_2,\quad\mathfrak{m}=0,1,2,...,\mathbb{M},$$

which shows that the numerical scheme is conditionally stable.

4. Convergence analysis

To describe convergence analysis, we first go through some important findings.

Theorem 4.1. *Note that $s(\varepsilon,\wp)\in C^4[\dot{a},\dot{b}]$, $\mathfrak{x}\in C^2[\dot{a},\dot{b}]$ such that $[\dot{a},\dot{b}]$ is partitioned with step length $\mathfrak{h}$ at the equidistant knots. If the trigonometric cubic B-spline approximation for solving TFGDE at knots $\varepsilon_0,...,\varepsilon_{\mathbb{L}}\in[\dot{a},\dot{b}]$ is $\mathbb{S}(\varepsilon,\wp)$, then there are δ that are free of $\mathfrak{h}$, such that*

$$\|\mathfrak{D}^k(s(\varepsilon,\wp)-\mathbb{S}(\varepsilon,\wp))\|_\infty\leq\delta_k\mathfrak{h}^{4-k},\ \ k=0,1,2. \tag{4.1}$$

Lemma 4.1. *The trigonometric cubic B-spline basis $\{\mathbb{T}_{-1},\mathbb{T}_0,...,\mathbb{T}_{\mathbb{L}+1}\}$ explained in Eq (2.8) follow the result [25]*

$$\sum_{\mathfrak{l}=-1}^{\mathbb{L}+1}|\mathbb{T}_{\mathfrak{l}}(\varepsilon)|\leq 6,\quad 0\leq\varepsilon\leq 1. \tag{4.2}$$

Theorem 4.2. *Let $\mathbb{S}(\varepsilon,\wp)$ be the computed solution to the exact solution $s(\varepsilon,\wp)$ for TFGDE. Furthermore, if $\mathfrak{x}\in C^2[0,1]$, we have*

$$\|s(\varepsilon,\wp)-\mathbb{S}(\varepsilon,\wp)\|_\infty\leq\mathfrak{O}\mathfrak{h}^2, \tag{4.3}$$

for every $\wp\geq 0$ and sufficiently small $\mathfrak{h}$, where $\mathfrak{O}$ is a positive constant free of $\mathfrak{h}$.

Proof. Suppose that $\check{S}(\varepsilon,\wp)=\sum_{\mathfrak{l}=-1}^{\mathbb{L}+1}\mathfrak{d}_{\mathfrak{l}}^{\mathfrak{m}}\mathbb{T}_{\mathfrak{l}}$ is the decisive solution to $\mathbb{S}(\varepsilon,\wp)$. Allow the current approach for solving TFGDE to achieve the following collocation conditions:

$$Ls(\varepsilon_{\mathfrak{l}},\wp)=L\mathbb{S}(\varepsilon_{\mathfrak{l}},\wp)=\mathfrak{x}(\varepsilon_{\mathfrak{l}},\wp),\quad \mathfrak{l}=0,1,...,\mathbb{L},$$

$$L\check{S}(\varepsilon_{\mathfrak{l}},\wp)=\check{\mathfrak{x}}(\varepsilon,\wp),\quad \mathfrak{l}=0,1,...,\mathbb{L}.$$

The error equation of trigonometric cubic B-spline method for TFGDE at $\mathfrak{m}$th time level, can be declared as

$$\begin{aligned}
&\Big(\mathrm{Im}\chi_1-\mathfrak{C}\varnothing\chi_3-\mathfrak{I}(1-\varnothing)\chi_1\Big)\Pi_{\mathfrak{l}-1}^{\mathfrak{m}+1}+\Big(\mathrm{Im}\chi_2-\mathfrak{I}(1-\varnothing)\chi_2\Big)\Pi_{\mathfrak{l}}^{\mathfrak{m}+1}\\
&+\Big(\mathrm{Im}\chi_1+\mathfrak{C}\varnothing\chi_3-\mathfrak{I}(1-\varnothing)\chi_1\Big)\Pi_{\mathfrak{l}+1}^{\mathfrak{m}+1}\\
&=\mathrm{Im}\chi_1\Pi_{\mathfrak{l}-1}^{\mathfrak{m}}+\mathrm{Im}\chi_2\Pi_{\mathfrak{l}}^{\mathfrak{m}}+\mathrm{Im}\chi_1\Pi_{\mathfrak{l}+1}^{\mathfrak{m}}-\mathrm{Im}\sum_{\varphi=1}^{\mathfrak{m}}\mathfrak{r}_\varphi\Big[\chi_1(\Pi_{\mathfrak{l}-1}^{\mathfrak{m}-\varphi+1}-\Pi_{\mathfrak{l}-1}^{\mathfrak{m}-\varphi})\\
&+\chi_2(\Pi_{\mathfrak{l}}^{\mathfrak{m}-\varphi+1}-\Pi_{\mathfrak{l}}^{\mathfrak{m}-\varphi})+\chi_1(\Pi_{\mathfrak{l}+1}^{\mathfrak{m}-\varphi+1}-\Pi_{\mathfrak{l}+1}^{\mathfrak{m}-\varphi})\Big]+\frac{1}{\mathfrak{h}}(\check{\mathfrak{x}}_{\mathfrak{l}}^{\mathfrak{m}+1}-\mathfrak{x}_{\mathfrak{l}}^{\mathfrak{m}+1}),
\end{aligned}\tag{4.4}$$

following the end conditions:

$$\chi_1\Pi_{\mathfrak{l}-1}^{\mathfrak{m}+1}+\chi_2\Pi_{\mathfrak{l}}^{\mathfrak{m}+1}+\chi_1\Pi_{\mathfrak{l}+1}^{\mathfrak{m}+1}=0,\ \ \mathfrak{l}=0,\mathbb{L},$$

where

$$\Pi_{\mathfrak{l}}^{\mathfrak{m}}=\mathfrak{d}_{\mathfrak{l}}^{\mathfrak{m}}-\aleph_{\mathfrak{l}}^{\mathfrak{m}},\ \ \mathfrak{l}=-1,0,1,...,\mathbb{L}+1.$$

From Theorem 4.1, we can see that

$$|\mho_{\mathfrak{l}}^{\mathfrak{m}}|=\mathfrak{h}\Big|\check{\mathfrak{x}}_{\mathfrak{l}}^{\mathfrak{m}}-\mathfrak{x}_{\mathfrak{l}}^{\mathfrak{m}}\Big|\leq\delta_0\mathfrak{h}^4.$$

Define $\mathfrak{V}^{\mathfrak{m}} = \max\{|\mathfrak{V}_{\mathfrak{l}}^{\mathfrak{m}}|; 0 \leq \mathfrak{l} \leq \mathbb{L}\}$, $\mathbb{R}_{\mathfrak{l}}^{\mathfrak{m}} = |\Pi_{\mathfrak{l}}^{\mathfrak{m}}|$ and $\mathbb{R}^{\mathfrak{m}} = \max\{|\Pi_{\mathfrak{l}}^{\mathfrak{m}}|; 0 \leq \mathfrak{l} \leq \mathbb{L}\}$. For $\mathfrak{m} = 0$ in Eq (4.4), we have

$$\begin{aligned}
&\Big(\operatorname{Im}\chi_1 - \mathfrak{C}\varnothing\chi_3 - \mathfrak{I}(1-\varnothing)\chi_1\Big)\Pi_{\mathfrak{l}-1}^1 + \Big(\operatorname{Im}\chi_2 - \mathfrak{I}(1-\varnothing)\chi_2\Big)\Pi_{\mathfrak{l}}^1 \\
&+\Big(\operatorname{Im}\chi_1 + \mathfrak{C}\varnothing\chi_3 - \mathfrak{I}(1-\varnothing)\chi_1\Big)\Pi_{\mathfrak{l}+1}^1 \\
=&\Big(\operatorname{Im}\chi_1\Pi_{\mathfrak{l}-1}^0 + \operatorname{Im}\chi_2\Pi_{\mathfrak{l}}^0 + \operatorname{Im}\chi_1\Pi_{\mathfrak{l}+1}^0\Big) + \frac{1}{\mathfrak{h}}\mathfrak{V}_{\mathfrak{l}}^1.
\end{aligned}$$

This implies

$$\begin{aligned}
&\Big(\operatorname{Im}\chi_2 - \mathfrak{I}(1-\varnothing)\chi_2\Big)\Pi_{\mathfrak{l}}^1 \\
&= -\Big[\Big(\operatorname{Im}\chi_1 - \mathfrak{C}\varnothing\chi_3 - \mathfrak{I}(1-\varnothing)\chi_1\Big)\Pi_{\mathfrak{l}-1}^1 + \Big(\operatorname{Im}\chi_1 + \mathfrak{C}\varnothing\chi_3 - \mathfrak{I}(1-\varnothing)\chi_1\Big)\Pi_{\mathfrak{l}+1}^1\Big] + \frac{1}{\mathfrak{h}}\mathfrak{V}_{\mathfrak{l}}^1.
\end{aligned}$$

From the initial condition $\mathbb{R}^0 = 0$ and taking absolute values of $\mathfrak{V}^1$ and $\Pi_{\mathfrak{l}}^1$ with a sufficiently small mesh size $\mathfrak{h}$, we have

$$\mathbb{R}_{\mathfrak{l}}^1 \leq \delta_{\mathfrak{l}}^1\mathfrak{h}^2.$$

Also from the boundary conditions, we obtain

$$\mathbb{R}^1 \leq \delta^1\mathfrak{h}^2. \tag{4.5}$$

Using the induction technique, we can easily prove that

$$\mathbb{R}_{\mathfrak{l}}^{\mathfrak{m}+1} \leq \delta\mathfrak{h}^2, \quad \forall \quad \mathfrak{m}, \tag{4.6}$$

where δ is a constant.

Hence, we can write

$$\check{S}(\varepsilon,\wp) - \mathbb{S}(\varepsilon,\wp) = \sum_{\mathfrak{l}=-1}^{\mathbb{L}+1}(\eth_{\mathfrak{l}}^{\mathfrak{m}} - \aleph_{\mathfrak{l}}^{\mathfrak{m}})\mathbb{T}_{\mathfrak{l}}(\varepsilon) \leq 6\delta\mathfrak{h}^2. \tag{4.7}$$

By means of triangular inequality, we have

$$\|s(\varepsilon,\wp) - \mathbb{S}(\varepsilon,\wp)\|_\infty \leq \|s(\varepsilon,\wp) - \check{S}(\varepsilon,\wp)\|_\infty + \|\check{S}(\varepsilon,\wp) - \mathbb{S}(\varepsilon,\wp)\|_\infty. \tag{4.8}$$

By using inequalities (4.1) and (4.7), we obtain

$$\|s(\varepsilon,\wp) - \mathbb{S}(\varepsilon,\wp)\|_\infty \leq \delta_0\mathfrak{h}^4 + 6\delta\mathfrak{h}^2 = \mathfrak{O}\mathfrak{h}^2, \tag{4.9}$$

where $\mathfrak{O} = \delta_0\mathfrak{h}^2 + 6\delta$. □

Hence, $\|s(\varepsilon,\wp) - \mathbb{S}(\varepsilon,\wp)\|_\infty \leq \mathfrak{O}\mathfrak{h}^2 + \mathrm{Re}_s(\Delta\wp)^{2-\mathfrak{B}}$, where $\mathfrak{O}$ and Re_s are constants.

5. Results and discussions

In this section, to demonstrate the efficiency and accuracy of the suggested approach, four numerical examples are investigated. Numerical findings are compared with existing methods available in literature as well as with the exact solutions for various nodal points $\varepsilon_{\mathfrak{l}}$ at some time levels $\wp^{\mathfrak{m}}$ employing the specific mesh size $\mathfrak{h}$ and time step $\Delta\wp$. The numerical simulation has been executed in Mathematica 12. In order to compute the maximum and Euclidean error norms for the proposed scheme, we use the following formulas:

$$\mathrm{L}_\infty = \max_{1\le \mathfrak{l}\le \mathbb{L}+1} |s(\varepsilon_{\mathfrak{l}}, \wp) - \mathbb{S}(\varepsilon_{\mathfrak{l}}, \wp)|,$$

$$\mathrm{L}_2 = \sqrt{\mathfrak{h}\sum_{\mathfrak{l}=1}^{\mathbb{L}+1} |s(\varepsilon_{\mathfrak{l}}, \wp) - \mathbb{S}(\varepsilon_{\mathfrak{l}}, \wp)|^2}.$$

The experimental order of convergence is calculated as

$$\mathrm{EOC} = \frac{1}{\log 2}\left[\log\left(\frac{\mathrm{L}_\infty(\mathbb{L})}{\mathrm{L}_\infty(2\mathbb{L})}\right)\right].$$

Example 5.1. Consider the following time fractional gas dynamics equation of the form [13]:

$$^{\mathrm{LC}}\mathfrak{D}^{\mathfrak{B}}_{\wp} s(\varepsilon, \wp) + s(\varepsilon, \wp)\frac{\partial s(\varepsilon, \wp)}{\partial \varepsilon} = s(\varepsilon, \wp)(1 - s(\varepsilon, \wp)), \quad 0 < \mathfrak{B} \le 1, \tag{5.1}$$

$$s(\varepsilon, 0) = e^{-\varepsilon}, \quad \varepsilon \in [0, 1],$$

$$s(0, \wp) = E_{\mathfrak{B}}(\wp^{\mathfrak{B}}), \; s(1, \wp) = e^{-1}E_{\mathfrak{B}}(\wp^{\mathfrak{B}}), \quad \wp \in [0, \mathfrak{T}],$$

where $E_{\mathfrak{B}}$ is the Mittag–Leffler function defined as

$$E_{\mathfrak{B}}(\wp) = \sum_{k=0}^{\infty} \frac{\wp^k}{\Gamma(\mathfrak{B}k + 1)}.$$

The exact solution to the problem is

$$s(\varepsilon, \wp) = e^{-\varepsilon}E_{\mathfrak{B}}(\wp^{\mathfrak{B}}).$$

We implement the scheme (2.12) to Example 5.1 to get the computational solution. In Tables 1 and 2, a comparison of error norms with those in [13] and [14] is presented. We have obtained a better accuracy compared to other methods. The experimental order of convergence and the CPU time taken in the computation of the numerical results by our proposed technique are tabulated in Table 3. The piece-wise defined spline solution at $\wp = 1$ for $\mathbb{L} = 100$, $\Delta\wp = 0.01$ is given in Eq (5.2). The exact and approximate solutions for various fractional orders $\mathfrak{B}$ are presented in Table 4.

Table 1. A comparison of error norms L_∞ and L_2 for Example 5.1 with other studies when $\mathbb{L} = 80$, $\wp = 1$ and $\mathfrak{B} = 0.50$.

$\Delta\wp$	[13]		[14]		Proposed method	
	L_∞	L_2	L_∞	L_2	L_∞	L_2
0.01	1.17815×10^{-2}	7.40766×10^{-3}	3.55659×10^{-3}	1.73903×10^{-3}	6.02036×10^{-4}	3.79089×10^{-4}
0.005	5.95821×10^{-3}	3.74342×10^{-3}	1.79622×10^{-3}	0.87334×10^{-3}	3.60322×10^{-4}	2.36533×10^{-4}
0.001	1.21004×10^{-3}	0.76063×10^{-3}	0.36364×10^{-3}	0.17680×10^{-3}	8.85761×10^{-5}	6.04303×10^{-5}
0.0005	0.60734×10^{-3}	0.38182×10^{-3}	0.18241×10^{-3}	0.08871×10^{-3}	4.63123×10^{-5}	3.18181×10^{-5}

Table 2. A comparison of error norms L_∞ and L_2 for Example 5.1 with other studies at various time knots when $\mathbb{L} = 80$, $\Delta\wp = 0.0005$ and $\mathfrak{B} = 0.50$.

$\wp$	[13]		[14]		Proposed method	
	L_∞	L_2	L_∞	L_2	L_∞	L_2
0.2	0.87075×10^{-3}	0.50233×10^{-3}	0.46167×10^{-3}	0.23390×10^{-3}	3.87462×10^{-4}	2.32251×10^{-4}
0.4	0.75565×10^{-3}	0.46757×10^{-3}	0.29086×10^{-3}	0.13289×10^{-3}	2.07185×10^{-4}	1.30055×10^{-4}
0.6	0.70014×10^{-3}	0.43899×10^{-3}	0.22388×10^{-3}	0.10435×10^{-3}	1.26823×10^{-4}	8.59606×10^{-5}
0.8	0.65152×10^{-3}	0.40981×10^{-3}	0.19676×10^{-3}	0.09402×10^{-3}	7.75223×10^{-5}	5.29422×10^{-5}

Table 3. Order of convergence for Example 5.1 when $\wp = 1$ and $\Delta\wp = 0.01$.

$\mathbb{L}$	L_∞	EOC	CPU time (s)
10	0.0213314	–	0.23437
20	0.00685282	1.63821	0.35937
40	0.002176118	1.65494	0.73437
80	0.0006880981	1.66107	1.6875

Table 4. Exact and approximate solutions when $\mathbb{L} = 100$, $\wp = 1$ and $\Delta\wp = 0.01$ for Example 5.1 for different fractional orders.

ε	$\mathfrak{B} = 0.25$		$\mathfrak{B} = 0.50$		$\mathfrak{B} = 0.75$	
	Exact	Approximate	Exact	Approximate	Exact	Approximate
0.0	9.55411	9.55411	5.00898	5.00898	3.48587	3.48587
0.1	8.64491	8.64492	4.53231	4.53234	3.15414	3.15421
0.2	7.82224	7.82225	4.10101	4.10106	2.85399	2.85410
0.3	7.07786	7.07787	3.71074	3.71082	2.58239	2.58255
0.4	6.40431	6.40433	3.35762	3.35770	2.33665	2.33683
0.5	5.79486	5.79488	3.03810	3.03819	2.11428	2.11448
0.6	5.24341	5.24342	2.74899	2.74907	1.91308	1.91328
0.7	4.74443	4.74444	2.48739	2.48746	1.73103	1.73120
0.8	4.29294	4.29295	2.25068	2.25074	1.5663	1.56643
0.9	3.88441	3.88442	2.0365	2.03654	1.41725	1.41732
1.0	3.51476	3.51476	1.84270	1.84270	1.28238	1.28238
L_∞		1.59262×10^{-4}		6.02748×10^{-4}		3.74731×10^{-4}
L_2		1.08097×10^{-4}		3.79101×10^{-4}		1.55645×10^{-4}

Figure 1 graphically illustrates the behavior of the approximated and exact solutions at different time levels. We observe a significant change in solution profiles when $\wp$ is changed and $\mathbb{L}$, $\Delta\wp$ and $\mathfrak{B}$ are fixed. This figure indicates that the magnitude of $s(\varepsilon, \wp)$ increases by increasing $\wp$. The graphs of both solutions are in excellent accordance. Figures 2 and 3 demonstrate an excellent 3D behavior of

exact and numerical solutions at time $\wp = 1$. It is clear that the numerical solution is consistent with the exact solution, which indicates effectiveness of the proposed method. Figure 4 displays the effect of fractional parameter $\mathfrak{B}$ on the computational solution by considering $\wp = 0.5$, $\mathbb{L} = 100$ and $\Delta\wp = 0.01$. We notice that as the value of the fractional parameter increases, we get closer to our exact solution.

The piece-wise defined spline solution for Example 5.1 at $\wp = 1$, $\mathbb{L} = 100$ and $\Delta\wp = 0.01$ is given as

$$\mathbb{S}(\varepsilon, 1) = \begin{cases} -10.0267\cos\frac{\varepsilon}{2} + 15.0357\cos\left(\frac{\varepsilon}{2}\right)^3 + 2421.15\sin\left(\frac{\varepsilon}{2}\right)^3 + \\ \sin\left(\frac{\varepsilon}{2}\right)(7253.44 - 22.5536\sin\varepsilon) - 1815.87\sin\varepsilon^2, & \text{if } \varepsilon \in [0, \frac{1}{100}], \\ 62.7016\cos\frac{\varepsilon}{2} - 57.6902\cos\left(\frac{\varepsilon}{2}\right)^3 - 2426.87\sin\left(\frac{\varepsilon}{2}\right)^3 + \\ 1820.16\csc\frac{\varepsilon}{2}\sin\varepsilon^2 + \sin\frac{\varepsilon}{2}(-7292.1 + 86.5353\sin\varepsilon), & \text{if } \varepsilon \in [\frac{1}{100}, \frac{2}{100}], \\ -82.8888\cos\frac{\varepsilon}{2} + 87.8808\cos\left(\frac{\varepsilon}{2}\right)^3 + 2424.04\sin\left(\frac{\varepsilon}{2}\right)^3 + \\ \sin\frac{\varepsilon}{2}(7266.46 - 131.821\sin\varepsilon) - 1818.03\csc\frac{\varepsilon}{2}\sin\varepsilon^2, & \text{if } \varepsilon \in [\frac{2}{100}, \frac{3}{100}], \\ \quad\vdots \qquad\qquad\qquad \vdots \qquad\qquad\qquad \vdots & \\ 1792.06\cos\frac{\varepsilon}{2} - 1644.31\cos\left(\frac{\varepsilon}{2}\right)^3 - 1788.96\sin\left(\frac{\varepsilon}{2}\right)^3 + \\ 1341.72\csc\frac{\varepsilon}{2}\sin\varepsilon^2 + \sin\frac{\varepsilon}{2}(-7071.92 + 2466.46\sin\varepsilon), & \text{if } \varepsilon \in [\frac{49}{100}, \frac{50}{100}], \\ -1810.87\cos\frac{\varepsilon}{2} + 1664.59\cos\left(\frac{\varepsilon}{2}\right)^3 + 1762.89\sin\left(\frac{\varepsilon}{2}\right)^3 + \\ \sin\frac{\varepsilon}{2}(7038.33 - 2496.88\sin\varepsilon) - 1322.17\csc\frac{\varepsilon}{2}\sin\varepsilon^2, & \text{if } \varepsilon \in [\frac{50}{100}, \frac{51}{100}], \\ \quad\vdots \qquad\qquad\qquad \vdots \qquad\qquad\qquad \vdots & \\ 2955.59\cos\frac{\varepsilon}{2} - 2087.9\cos\left(\frac{\varepsilon}{2}\right)^3 - 225.767\sin\left(\frac{\varepsilon}{2}\right)^3 + \\ 169.326\csc\frac{\varepsilon}{2}\sin\varepsilon^2 + \sin\frac{\varepsilon}{2}(-5568.02 + 3131.85\sin\varepsilon), & \text{if } \varepsilon \in [\frac{97}{100}, \frac{98}{100}], \\ -2955.\cos\frac{\varepsilon}{2} + 2077.18\cos\left(\frac{\varepsilon}{2}\right)^3 + 195.485\sin\left(\frac{\varepsilon}{2}\right)^3 + \\ \sin\frac{\varepsilon}{2}(5513.18 - 3115.77\sin\varepsilon) - 146.614\csc\frac{\varepsilon}{2}\sin\varepsilon^2, & \text{if } \varepsilon \in [\frac{98}{100}, \frac{99}{100}], \\ 2975.85\cos\frac{\varepsilon}{2} - 2069.23\cos\left(\frac{\varepsilon}{2}\right)^3 - 161.137\sin\left(\frac{\varepsilon}{2}\right)^3 + \\ 120.853\csc\frac{\varepsilon}{2}\sin\varepsilon^2 + \sin\frac{\varepsilon}{2}(-5473.36 + 3103.85\sin\varepsilon), & \text{if } \varepsilon \in [\frac{99}{100}, 1]. \end{cases} \tag{5.2}$$

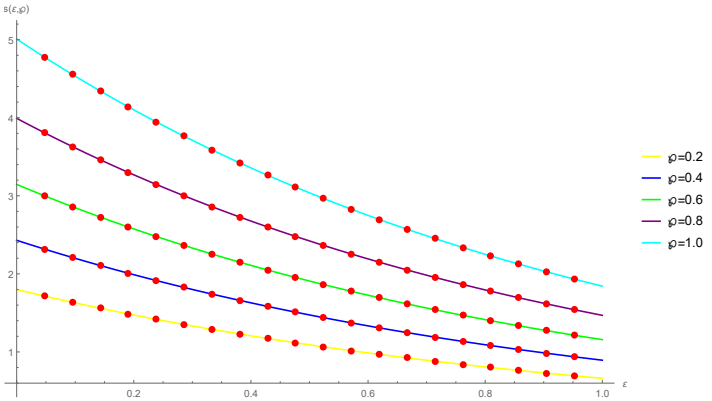

Figure 1. Plot showing exact and approximate solutions when $\mathbb{L} = 100$, $\Delta\wp = 0.01$ and $\mathfrak{B} = 0.50$ at various time levels.

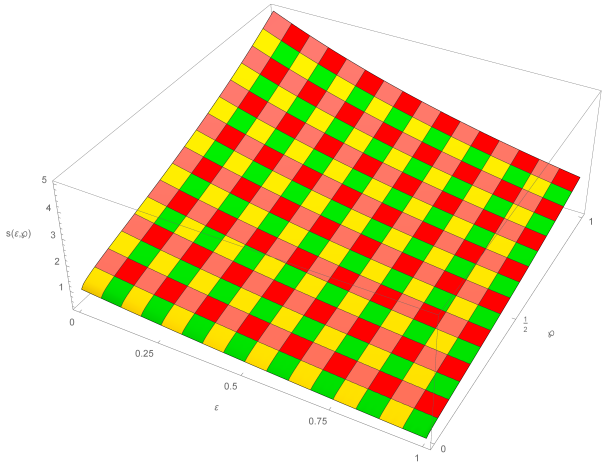

Figure 2. Three-dimensional plot of exact solutions for Example 5.1 when $\mathbb{L} = 100$, $\Delta\wp = 0.01$ and $\mathfrak{B} = 0.50$.

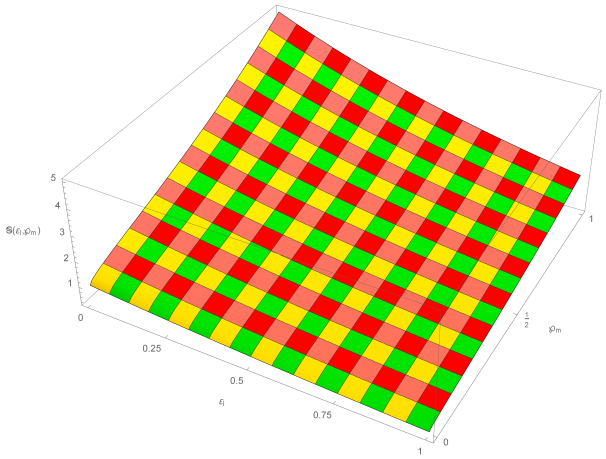

Figure 3. Three-dimensional plot of numerical results for Example 5.1 when $\mathbb{L} = 100$, $\Delta\wp = 0.01$ and $\mathfrak{B} = 0.50$.

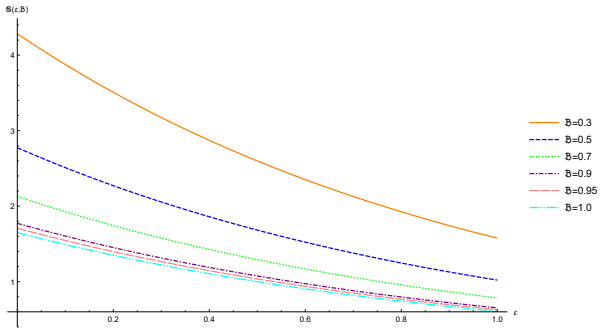

Figure 4. The effect of fractional parameter $\mathfrak{B}$ on the computational solution for Example 5.1 when $\wp = 0.5$, $\mathbb{L} = 100$ and $\Delta\wp = 0.01$.

Example 5.2. Consider the following time fractional gas dynamics equation of the form [6]:

$$^{\mathbf{LC}}\mathfrak{D}_{\wp}^{\mathfrak{B}}s(\varepsilon,\wp)+s(\varepsilon,\wp)\frac{\partial s(\varepsilon,\wp)}{\partial\varepsilon}=s(\varepsilon,\wp)(1-s(\varepsilon,\wp))-e^{\wp-\varepsilon},\ \ 0<\mathfrak{B}\leq 1,\ \ \wp>0, \tag{5.3}$$

$$s(\varepsilon,0)=1-e^{-\varepsilon},\ \ \varepsilon\in[0,1],$$

$$s(0,\wp)=-\wp^{\mathfrak{B}}E_{1,\mathfrak{B}+1}(\wp),\ s(1,\wp)=1-e^{-1}-e^{-1}\wp^{\mathfrak{B}}E_{1,\mathfrak{B}+1}(\wp),\ \ \wp\in[0,\mathfrak{T}],$$

where $E_{\mathfrak{B},\alpha}$ is the two-parametric Mittag–Leffler function defined as

$$E_{\mathfrak{B},\alpha}(\wp)=\sum_{k=0}^{\infty}\frac{\wp^k}{\Gamma(\mathfrak{B}k+\alpha)}.$$

The exact solution to the problem is

$$s(\varepsilon,\wp)=1-e^{-\varepsilon}-e^{-\varepsilon}\wp^{\mathfrak{B}}E_{1,\mathfrak{B}+1}(\wp).$$

Table 5 reports the error norms for different values of fractional parameter $\mathfrak{B}$ at $\wp=1$ and $\mathbb{L}=100$. Table 6 presents the error norms at various time knots and for different step sizes when $\mathfrak{B}=0.50$. Exact and computational outcomes for various values of fractional parameter $\mathfrak{B}$ when $\mathbb{L}=100$, $\wp=1$ and $\Delta\wp=0.01$ are tabulated in Table 7. It is observed that the computational and exact solutions are in good agreement. The piece-wise defined spline solution for Example 5.2 at $\wp=1$, $\mathbb{L}=100$ and $\Delta\wp=0.01$ is given in Eq (5.4). Table 8 presents the comparison of error norms with the method discussed in [6] at different time knots and fractional orders. From this table, the efficiency of the proposed method is remarkably pronounced. It is observed that the error norms of the present method are less than those computed from the semi-analytical solution derived in [6].

Table 5. Maximum error norms L_∞ and Euclidean error norms L_2 when $\mathbb{L}=100$, $\wp=1$ for Example 5.2 corresponding to different fractional orders.

$\Delta\wp$	$\mathfrak{B}=0.25$		$\mathfrak{B}=0.50$		$\mathfrak{B}=0.75$	
	L_∞	L_2	L_∞	L_2	L_∞	L_2
0.01	3.69844×10^{-3}	2.47623×10^{-3}	4.54598×10^{-3}	2.93294×10^{-3}	2.21600×10^{-3}	1.52382×10^{-3}
0.005	1.91491×10^{-3}	1.28204×10^{-3}	2.41824×10^{-3}	1.58057×10^{-3}	1.44097×10^{-3}	1.03372×10^{-3}
0.001	3.97575×10^{-4}	2.66275×10^{-4}	5.22475×10^{-4}	3.46776×10^{-4}	4.55943×10^{-4}	3.05383×10^{-4}
0.0005	2.00173×10^{-4}	1.34092×10^{-4}	2.67174×10^{-4}	1.77002×10^{-4}	2.56362×10^{-4}	1.68682×10^{-4}

Table 6. Maximum error norm L_∞ and Euclidean error norm L_2 at various time levels when $\mathfrak{B}=0.50$ for Example 5.2.

$\mathfrak{h}=\Delta\wp$	$\wp=0.2$		$\wp=0.4$		$\wp=0.6$		$\wp=0.8$	
	L_∞	L_2	L_∞	L_2	L_∞	L_2	L_∞	L_2
$\frac{1}{100}$	1.17673×10^{-2}	5.17553×10^{-3}	8.08584×10^{-3}	4.0544×10^{-3}	6.35047×10^{-3}	3.54398×10^{-3}	5.21918×10^{-3}	3.21038×10^{-3}
$\frac{1}{120}$	9.87829×10^{-3}	4.34265×10^{-3}	6.80441×10^{-3}	3.4097×10^{-3}	5.36286×10^{-3}	2.98976×10^{-3}	4.42947×10^{-3}	2.71966×10^{-3}
$\frac{1}{140}$	8.5147×10^{-3}	3.74193×10^{-3}	5.87618×10^{-3}	2.9432×10^{-3}	4.64379×10^{-3}	2.58691×10^{-3}	3.85015×10^{-3}	2.36102×10^{-3}
$\frac{1}{160}$	7.48358×10^{-3}	3.28796×10^{-3}	5.17236×10^{-3}	2.58977×10^{-3}	4.09641×10^{-3}	2.28063×10^{-3}	3.4066×10^{-3}	2.08689×10^{-3}
$\frac{1}{180}$	6.67627×10^{-3}	2.93269×10^{-3}	4.62012×10^{-3}	2.31262×10^{-3}	3.66554×10^{-3}	2.03978×10^{-3}	3.05585×10^{-3}	1.87054×10^{-3}

Table 7. Exact and numerical outcomes when $\mathbb{L} = 100$, $\wp = 1$ and $\Delta\wp = 0.01$ for Example 5.2.

ε	$\mathfrak{B} = 0.25$		$\mathfrak{B} = 0.50$		$\mathfrak{B} = 0.75$	
	Exact	Numerical	Exact	Numerical	Exact	Numerical
0.0	−2.53365	−2.53365	−2.2907	−2.2907	−2.01147	−2.01147
0.1	−2.19738	−2.19756	−1.97755	−1.97783	−1.72489	−1.72506
0.2	−1.89311	−1.89345	−1.6942	−1.69474	−1.46559	−1.46592
0.3	−1.61779	−1.61827	−1.43781	−1.4386	−1.23096	−1.23146
0.4	−1.36868	−1.36926	−1.20582	−1.20683	−1.01865	−1.01934
0.5	−1.14327	−1.14393	−0.995909	−0.997117	−0.826551	−0.827426
0.6	−0.93931	−0.940017	−0.805973	−0.807343	−0.652732	−0.6538
0.7	−0.75476	−0.755462	−0.634112	−0.635586	−0.495454	−0.496713
0.8	−0.587773	−0.588396	−0.478606	−0.480066	−0.353143	−0.354546
0.9	−0.436676	−0.437101	−0.337898	−0.339028	−0.224374	−0.225679
1.0	−0.299958	−0.299958	−0.21058	−0.21058	−0.107859	−0.107859
L_∞		3.69844×10^{-3}		4.54598×10^{-3}		2.216×10^{-3}
L_2		2.47623×10^{-3}		2.93294×10^{-3}		1.52382×10^{-3}

Table 8. A comparison of error norms when $\mathfrak{h} = \Delta\wp = 0.01$ for Example 5.2.

$\wp$	$\mathfrak{B}$	[6]		Proposed method	
		L_∞	L_2	L_∞	L_2
0.2	0.5	1.42819×10^{-1}	9.45221×10^{-2}	1.17673×10^{-2}	5.17553×10^{-3}
	0.7	4.21493×10^{-2}	2.78958×10^{-2}	9.24571×10^{-3}	3.70292×10^{-3}
	0.9	6.85292×10^{-3}	4.53549×10^{-3}	2.7463×10^{-3}	9.75071×10^{-4}
0.5	0.5	2.81188×10^{-1}	1.861×10^{-1}	7.10279×10^{-3}	3.76407×10^{-3}
	0.7	1.14254×10^{-1}	7.56171×10^{-2}	6.28378×10^{-3}	3.12786×10^{-3}
	0.9	2.49654×10^{-2}	1.65229×10^{-2}	8.11543×10^{-4}	3.50029×10^{-4}
1	0.5	2.41329×10^{-1}	1.59719×10^{-1}	4.54598×10^{-3}	2.9329×10^{-3}
	0.7	1.43865×10^{-1}	9.52147×10^{-2}	3.04349×10^{-3}	2.18887×10^{-3}
	0.9	4.32218×10^{-2}	2.86057×10^{-2}	6.14144×10^{-4}	2.99519×10^{-4}

The effect of varying the time on exact and approximate solutions is sketched in Figure 5. It can be seen that an increase in time level leads to a decrease in $s(\varepsilon, \wp)$. Figures 6 and 7 display a three-dimensional visual of exact and numerical outcomes when $\mathbb{L} = 100$, $\Delta\wp = 0.01$ and $\mathfrak{B} = 0.50$. The influence of the fractional parameter on the computational solution is observed in Figure 8. We conclude that an increase in the fractional parameter leads to a closer approximation to the exact solution.

The piece-wise defined spline solution for Example 5.2 at $\wp = 1$, $\mathbb{L} = 100$ and $\Delta\wp = 0.01$ is given as

$$\mathbb{S}(\varepsilon,1)=\begin{cases}126.766\cos\frac{\varepsilon}{2}-129.057\cos\left(\frac{\varepsilon}{2}\right)^3-17494.7\sin\left(\frac{\varepsilon}{2}\right)^3+\\ 13121.0\sin\varepsilon^2+\sin\frac{\varepsilon}{2}(-52477.6+193.586\sin\varepsilon), & \text{if } \varepsilon\in[0,\frac{1}{100}],\\ -399.055\cos\frac{\varepsilon}{2}+396.746\cos\left(\frac{\varepsilon}{2}\right)^3+17556.2\sin\left(\frac{\varepsilon}{2}\right)^3+\\ \sin\frac{\varepsilon}{2}(52685.8-595.12\sin\varepsilon)-13167.2\csc\frac{\varepsilon}{2}\sin\varepsilon^2, & \text{if } \varepsilon\in[\frac{1}{100},\frac{2}{100}],\\ 656.344\cos\frac{\varepsilon}{2}-658.512\cos\left(\frac{\varepsilon}{2}\right)^3-17608.5\sin\left(\frac{\varepsilon}{2}\right)^3+\\ 13206.4\csc\frac{\varepsilon}{2}\sin\varepsilon^2+\sin\frac{\varepsilon}{2}(-52850.6+987.768\sin\varepsilon), & \text{if } \varepsilon\in[\frac{2}{100},\frac{3}{100}],\\ \quad\vdots \qquad\qquad \vdots \qquad\qquad \vdots\\ 15311.7\cos\frac{\varepsilon}{2}-14039.9\cos\left(\frac{\varepsilon}{2}\right)^3-14847.8\sin\left(\frac{\varepsilon}{2}\right)^3+\\ 11135.9\csc\frac{\varepsilon}{2}\sin\varepsilon^2+\sin\frac{\varepsilon}{2}(-59355.3+21059.8\sin\varepsilon), & \text{if } \varepsilon\in[\frac{49}{100},\frac{50}{100}],\\ -15651.1\cos\frac{\varepsilon}{2}+14296.2\cos\left(\frac{\varepsilon}{2}\right)^3+14668.5\sin\left(\frac{\varepsilon}{2}\right)^3+\\ \sin\frac{\varepsilon}{2}(59424.3-21444.3\sin\varepsilon)-11001.4\csc\frac{\varepsilon}{2}\sin\varepsilon^2, & \text{if } \varepsilon\in[\frac{50}{100},\frac{51}{100}],\\ \quad\vdots \qquad\qquad \vdots \qquad\qquad \vdots\\ -26946.2\cos\frac{\varepsilon}{2}+19061.7\cos\left(\frac{\varepsilon}{2}\right)^3+2070.91\sin\left(\frac{\varepsilon}{2}\right)^3+\\ \sin\frac{\varepsilon}{2}(50820.8-28592.5\sin\varepsilon)-1553.19\csc\frac{\varepsilon}{2}\sin\varepsilon^2, & \text{if } \varepsilon\in[\frac{97}{100},\frac{98}{100}],\\ 26844.8\cos\frac{\varepsilon}{2}-18843.8\cos\left(\frac{\varepsilon}{2}\right)^3-1762.82\sin\left(\frac{\varepsilon}{2}\right)^3+\\ 1322.11\csc\frac{\varepsilon}{2}\sin\varepsilon^2+\sin\frac{\varepsilon}{2}(-50026.9+28265.8\sin\varepsilon), & \text{if } \varepsilon\in[\frac{98}{100},\frac{99}{100}],\\ -26703.1\cos\frac{\varepsilon}{2}+18592.9\cos\left(\frac{\varepsilon}{2}\right)^3+1457.03\sin\left(\frac{\varepsilon}{2}\right)^3+\\ \sin\frac{\varepsilon}{2}(49167.5-27889.4\sin\varepsilon)-1092.77\csc\frac{\varepsilon}{2}\sin\varepsilon^2, & \text{if } \varepsilon\in[\frac{99}{100},1].\end{cases}\tag{5.4}$$

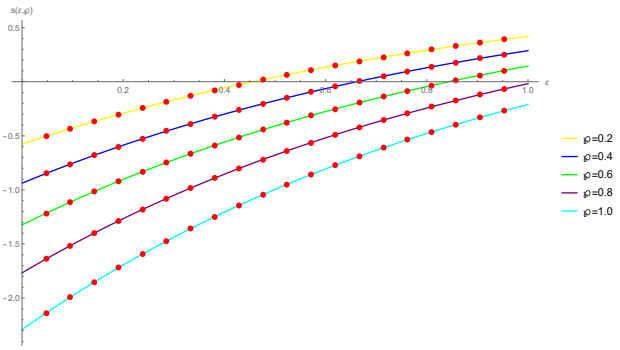

Figure 5. Plot of approximate and exact outcomes when $\mathbb{L}=100$, $\Delta_{\wp}=0.01$ and $\mathfrak{B}=0.50$.

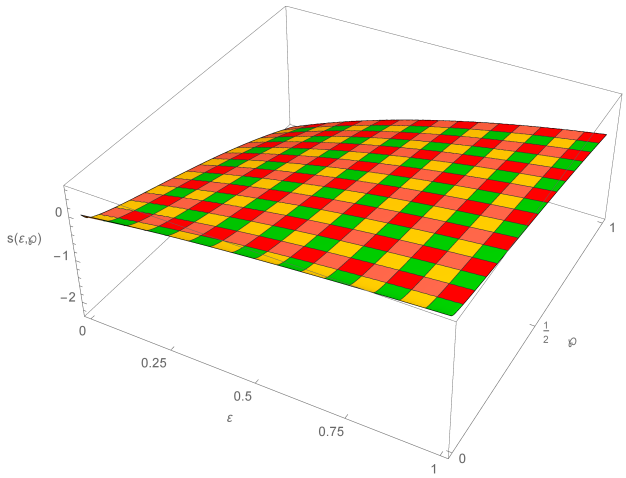

Figure 6. Three-dimensional view of exact solutions for Example 5.2 when $\mathbb{L} = 100$, $\Delta\wp = 0.01$ and $\mathfrak{B} = 0.50$.

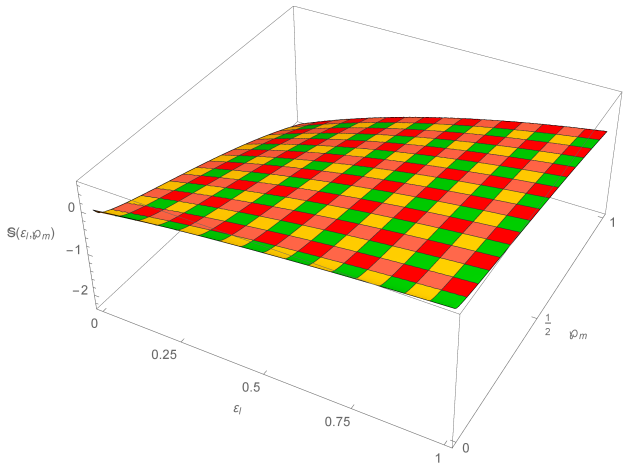

Figure 7. Three-dimensional view of numerical results for Example 5.2 when $\mathbb{L} = 100$, $\Delta\wp = 0.01$ and $\mathfrak{B} = 0.50$.

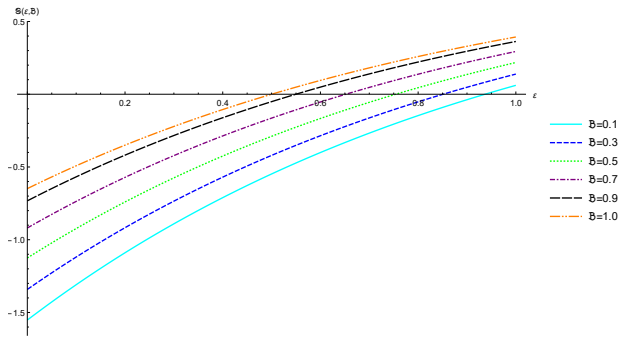

Figure 8. The effect of fractional order $\mathfrak{B}$ on the approximate solution for Example 5.2 when $\wp = 0.5$, $\mathbb{L} = 100$ and $\Delta\wp = 0.01$.

Example 5.3. Consider the following time fractional gas dynamics equation:

$$ {}^{\mathrm{LC}}\mathfrak{D}_{\wp}^{\mathfrak{B}} s(\varepsilon,\wp) + s(\varepsilon,\wp)\frac{\partial s(\varepsilon,\wp)}{\partial \varepsilon} = s(\varepsilon,\wp)(1-s(\varepsilon,\wp)) + \mathfrak{x}(\varepsilon,\wp), \quad 0 < \mathfrak{B} \leq 1, \quad \wp > 0, \tag{5.5} $$

$$ s(\varepsilon,0) = 0, \quad \varepsilon \in [0,1], $$

$$ s(0,\wp) = 0, s(1,\wp) = \wp^{\mathfrak{B}} \tan(1), \quad \wp \in [0,\mathfrak{T}], $$

where

$$ \mathfrak{x}(\varepsilon,\wp) = -\frac{\pi \csc \pi\mathfrak{B}}{\Gamma(-\mathfrak{B})} \tan\varepsilon + \wp^{2\mathfrak{B}} \tan\varepsilon \sec^2\varepsilon - \wp^{\mathfrak{B}} \tan\varepsilon + \wp^{2\mathfrak{B}} \tan^2\varepsilon. $$

The exact solution to the problem is

$$ s(\varepsilon,\wp) = \wp^{\mathfrak{B}} \tan\varepsilon. $$

In Table 9, the L_∞ and L_2 error norms are presented for various values of fractional parameter $\mathfrak{B}$ with $\wp = 1$ and $\mathbb{L} = 100$. For $\mathfrak{h} = \Delta\wp$ and at various time knots, error norms L_∞ and L_2 are computed in Table 10 for a fixed fractional order $\mathfrak{B} = 0.50$. We have compared the exact and numerical solutions for Example 5.3 for different values of fractional order $\mathfrak{B}$ in Table 11. In Table 12, the experimental order of convergence and CPU time in seconds is reported. The piece-wise spline solutions for Example 5.3 at $\wp = 1$, $\mathbb{L} = 100$ and $\Delta\wp = 0.01$ are given in Eq (5.5).

Table 9. Error norms L_∞ and L_2 for Example 5.3 when $\mathbb{L} = 100$, $\wp = 1$ for various fractional orders.

$\Delta\wp$	$\mathfrak{B} = 0.25$		$\mathfrak{B} = 0.50$		$\mathfrak{B} = 0.75$	
	L_∞	L_2	L_∞	L_2	L_∞	L_2
0.01	8.50403×10^{-4}	1.41383×10^{-4}	9.61123×10^{-4}	4.46289×10^{-4}	1.17661×10^{-3}	7.69718×10^{-4}
0.005	8.60954×10^{-4}	1.22026×10^{-4}	8.74341×10^{-4}	2.52383×10^{-4}	6.36569×10^{-4}	4.21379×10^{-4}
0.001	8.41729×10^{-4}	1.01507×10^{-4}	7.83217×10^{-4}	9.77376×10^{-5}	6.04633×10^{-4}	1.10021×10^{-4}
0.0005	8.35969×10^{-4}	9.95314×10^{-5}	7.69857×10^{-4}	8.63077×10^{-5}	6.01817×10^{-4}	7.65989×10^{-5}

Table 10. Error norms L_∞ and L_2 for Example 5.3 when $\mathfrak{B} = 0.50$ at different time knots.

$\mathfrak{h} = \Delta\wp$	$\wp = 0.2$		$\wp = 0.4$		$\wp = 0.6$		$\wp = 0.8$	
	L_∞	L_2	L_∞	L_2	L_∞	L_2	L_∞	L_2
$\frac{1}{100}$	7.07204×10^{-3}	3.49434×10^{-3}	2.94894×10^{-3}	1.70596×10^{-3}	1.62563×10^{-3}	9.96108×10^{-4}	1.01689×10^{-3}	6.42331×10^{-4}
$\frac{1}{120}$	6.0654×10^{-3}	2.99309×10^{-3}	2.522×10^{-3}	1.45871×10^{-3}	1.38865×10^{-3}	8.50993×10^{-4}	8.68347×10^{-4}	5.48019×10^{-4}
$\frac{1}{140}$	5.30865×10^{-3}	2.6179×10^{-3}	2.20325×10^{-3}	1.27426×10^{-3}	1.21215×10^{-3}	7.42935×10^{-4}	7.57773×10^{-4}	4.78002×10^{-4}
$\frac{1}{160}$	4.71981×10^{-3}	2.32666×10^{-3}	1.95621×10^{-3}	1.13143×10^{-3}	1.0756×10^{-3}	6.59358×10^{-4}	6.72287×10^{-4}	4.23956×10^{-4}
$\frac{1}{180}$	4.24883×10^{-3}	2.09406×10^{-3}	1.75928×10^{-3}	1.01756×10^{-3}	9.66858×10^{-4}	5.92788×10^{-4}	6.04223×10^{-4}	3.80968×10^{-4}

Table 11. Exact and numerical solutions for Example 5.3 for different values of $\mathfrak{B}$ when $\mathbb{L} = 100$, $\wp = 1$ and $\Delta\wp = 0.01$.

ε	$\mathfrak{B} = 0.25$	$\mathfrak{B} = 0.50$	$\mathfrak{B} = 0.75$	Exact solution
0.0	0.00000	0.00000	0.00000	0.00000
0.1	0.10025	0.10047	0.10075	0.10033
0.2	0.20263	0.20274	0.20293	0.20271
0.3	0.30925	0.30929	0.30937	0.30934
0.4	0.42270	0.42269	0.42269	0.42279
0.5	0.54621	0.54617	0.54612	0.54630
0.6	0.68405	0.68399	0.68391	0.68414
0.7	0.84221	0.84215	0.84207	0.84229
0.8	1.02958	1.02953	1.02946	1.02964
0.9	1.26013	1.26010	1.26005	1.26016
1.0	1.55741	1.55741	1.55741	1.55741

Table 12. Order of convergence for Example 5.3 when $\wp = 1$, $\Delta\wp = 0.001$ and $\mathfrak{B} = 0.95$.

$\mathbb{L}$	L_∞	EOC	CPU time (s)
5	0.0038709	–	0.92187
10	0.00135279	1.51673	1.42344
20	0.0004917785	1.45987	1.81094
40	0.00018486911	1.41150	2.38125

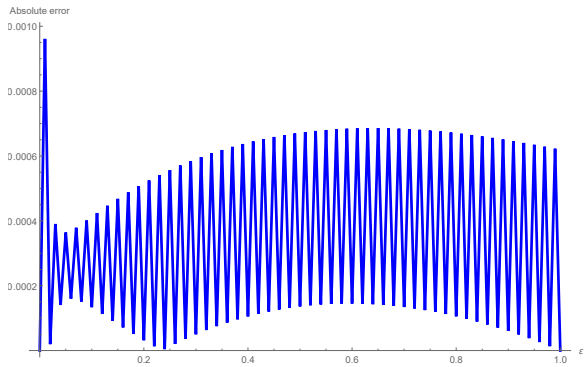

Figure 9. Absolute error plot when $\mathbb{L} = 100$, $\Delta\wp = 0.01$ and $\mathfrak{B} = 0.50$ for Example 5.3.

Figure 9 reflects the 2D absolute error profile for $\mathbb{L} = 100$, $\Delta\wp = 0.01$ and $\mathfrak{B} = 0.50$. This figure indicates the error at each point in space. Figure 10 exposes the graph of exact and approximate solutions when $\mathbb{L} = 100$, $\Delta\wp = 0.01$ and $\mathfrak{B} = 0.50$ at various time levels. This figure reveals a significant change in solution profiles with a change in time. We observe an increasing behavior

between time and solution profiles. Figures 11 and 12 show the close agreement of 3D plots for computational and exact solutions by taking $\mathbb{L} = 100$, $\Delta\wp = 0.01$ and $\mathfrak{B} = 0.50$. Approximate solutions for different values of fractional parameter $\mathfrak{B}$ and for $\wp = 0.5$, $\mathbb{L} = 100$ and $\Delta\wp = 0.01$ can be visualised in Figure 13. From this figure, it is evident that as we increase the fractional parameter, we get closer to the exact solution.

The piece-wise spline solution for Example 5.3 at $\wp = 1$ for $\mathbb{L} = 100$, $\Delta\wp = 0.01$ is given as

$$\mathbb{S}(\varepsilon, 1) = \begin{cases} 60.5372\cos\frac{\varepsilon}{2} - 60.5372\cos\left(\frac{\varepsilon}{2}\right)^3 - 3858.82\sin\left(\frac{\varepsilon}{2}\right)^3 + \\ 2894.11\sin\varepsilon^2 + \sin\frac{\varepsilon}{2}(-11575.5 + 90.8059\sin\varepsilon), & \text{if } \varepsilon \in [0, \frac{1}{100}], \\ 19.2917\cos\frac{\varepsilon}{2} - 19.2931\cos\left(\frac{\varepsilon}{2}\right)^3 - 1109.42\sin\left(\frac{\varepsilon}{2}\right)^3 + \\ 832.062\csc\frac{\varepsilon}{2}\sin\varepsilon^2 + \sin\frac{\varepsilon}{2}(-3326.44 + 28.9396\sin\varepsilon), & \text{if } \varepsilon \in [\frac{1}{100}, \frac{2}{100}], \\ -70.1482\cos\frac{\varepsilon}{2} + 70.1349\cos\left(\frac{\varepsilon}{2}\right)^3 + 1870.62\sin\left(\frac{\varepsilon}{2}\right)^3 + \\ \sin\frac{\varepsilon}{2}(5617.25 - 105.202\sin\varepsilon) - 1402.97\csc\frac{\varepsilon}{2}\sin\varepsilon^2, & \text{if } \varepsilon \in [\frac{2}{100}, \frac{3}{100}], \\ \quad\vdots \qquad\qquad\qquad \vdots \qquad\qquad\qquad \vdots & \\ -1606.64\cos\frac{\varepsilon}{2} + 1473.\cos\left(\frac{\varepsilon}{2}\right)^3 + 1558.73\sin\left(\frac{\varepsilon}{2}\right)^3 + \\ \sin\frac{\varepsilon}{2}(6232.54 - 2209.5\sin\varepsilon) - 1169.05\csc\frac{\varepsilon}{2}\sin\varepsilon^2, & \text{if } \varepsilon \in [\frac{49}{100}, \frac{50}{100}], \\ 1637.07\cos\frac{\varepsilon}{2} - 1495.53\cos\left(\frac{\varepsilon}{2}\right)^3 - 1533.44\sin\left(\frac{\varepsilon}{2}\right)^3 + \\ 1150.08\csc\frac{\varepsilon}{2}\sin\varepsilon^2 + \sin\frac{\varepsilon}{2}(-6210.99 + 2243.29\sin\varepsilon), & \text{if } \varepsilon \in [\frac{50}{100}, \frac{51}{100}], \\ \quad\vdots \qquad\qquad\qquad \vdots \qquad\qquad\qquad \vdots & \\ 3412.52\cos\frac{\varepsilon}{2} - 2412.92\cos\left(\frac{\varepsilon}{2}\right)^3 - 257.49\sin\left(\frac{\varepsilon}{2}\right)^3 + \\ 193.118\csc\frac{\varepsilon}{2}\sin\varepsilon^2 + \sin\frac{\varepsilon}{2}(-6423.07 + 3619.38\sin\varepsilon), & \text{if } \varepsilon \in [\frac{97}{100}, \frac{98}{100}], \\ -3506.36\cos\frac{\varepsilon}{2} + 2462.68\cos\left(\frac{\varepsilon}{2}\right)^3 + 235.624\sin\left(\frac{\varepsilon}{2}\right)^3 + \\ \sin\frac{\varepsilon}{2}(6548.49 - 3694.03\sin\varepsilon) - 176.718\csc\frac{\varepsilon}{2}\sin\varepsilon^2, & \text{if } \varepsilon \in [\frac{98}{100}, \frac{99}{100}], \\ 3513.63\cos\frac{\varepsilon}{2} - 2445.18\cos\left(\frac{\varepsilon}{2}\right)^3 - 186.488\sin\left(\frac{\varepsilon}{2}\right)^3 + \\ 139.866\csc\frac{\varepsilon}{2}\sin\varepsilon^2 + \sin\frac{\varepsilon}{2}(-6455.64 + 3667.76\sin\varepsilon), & \text{if } \varepsilon \in [\frac{99}{100}, 1]. \end{cases} \tag{5.6}$$

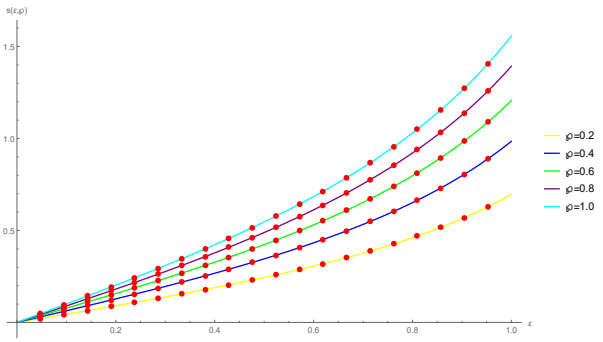

Figure 10. Graph representing numerical and exact outcomes for $\mathbb{L} = 100$, $\Delta\wp = 0.01$ and $\mathfrak{B} = 0.50$ at different time levels.

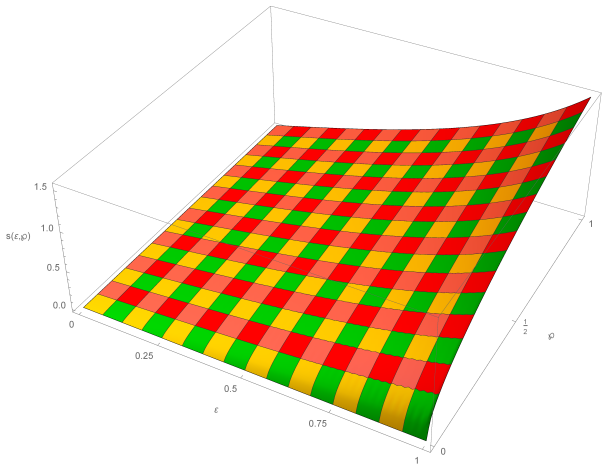

Figure 11. Three-dimensional view of exact solutions for Example 5.3 when $\mathbb{L} = 100$, $\Delta\wp = 0.01$ and $\mathfrak{B} = 0.50$.

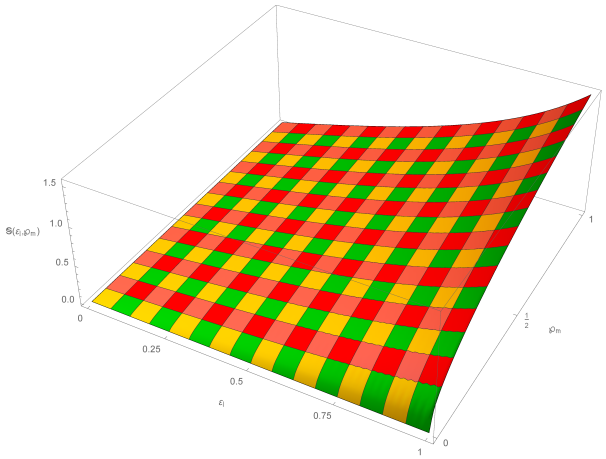

Figure 12. Three-dimensional view of numerical results for Example 5.3 when $\mathbb{L} = 100$, $\Delta\wp = 0.01$ and $\mathfrak{B} = 0.50$.

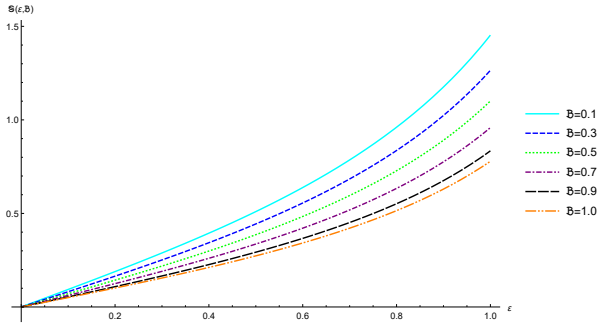

Figure 13. Approximate solutions for different $\mathfrak{B}$ at $\wp = 0.5$, $\mathbb{L} = 100$ and $\Delta\wp = 0.01$.

Example 5.4. Consider the following time fractional gas dynamics equation of the form:

$$ {}^{\mathrm{LC}}\mathfrak{D}_{\wp}^{\mathfrak{B}} s(\varepsilon,\wp) + s(\varepsilon,\wp)\frac{\partial s(\varepsilon,\wp)}{\partial \varepsilon} = s(\varepsilon,\wp)(1 - s(\varepsilon,\wp)) + \mathfrak{x}(\varepsilon,\wp), \quad 0 < \mathfrak{B} \leq 1, \quad \wp > 0, \tag{5.7} $$

$$ s(\varepsilon,0) = 0, \quad \varepsilon \in [0,1], $$

$$ s(0,\wp) = 0, s(1,\wp) = \wp^{2+\mathfrak{B}} \sin(\pi), \quad \wp \in [0,\mathfrak{T}], $$

where

$$ \mathfrak{x}(\varepsilon,\wp) = -\frac{\pi\wp^2 \csc(\pi\mathfrak{B})}{2\Gamma(-2-\mathfrak{B})}\sin(\pi\varepsilon) + \frac{\pi}{2}\wp^{4+2\mathfrak{B}}\sin(2\pi\varepsilon) - \wp^{2+\mathfrak{B}}\sin(\pi\varepsilon) + \wp^{4+2\mathfrak{B}}\sin^2(\pi\varepsilon). $$

The exact solution to the problem is

$$ s(\varepsilon,\wp) = \wp^{2+\mathfrak{B}}\sin(\pi\varepsilon). $$

Table 13 reports exact and computational outcomes for different values of fractional order $\mathfrak{B}$ when $\mathbb{L} = 100$, $\wp = 1$ and $\Delta\wp = 0.01$ at space knots. Error norms at various time knots and for different step sizes when $\mathfrak{B} = 0.50$ are tabulated in Table 14. The experimental order of convergence and CPU time in seconds is calculated and presented in Table 15. The piece-wise spline solutions at $\wp = 1$ for $\mathbb{L} = 100$, $\Delta\wp = 0.01$ are given in Eq (5.8). The effect of time on solution profiles for $\mathbb{L} = 100$, $\Delta\wp = 0.01$ and $\mathfrak{B} = 0.50$ is observed in Figure 14. This graph reveals an excellent analogy between the exact and numerical solutions, which indicates that the proposed method is effective. A close agreement between the 3D exact and approximate solutions at $\wp = 1$ is evident from Figures 15 and 16. The behavior of the fractional parameter on an approximate solution for Example 5.4 when $\wp = 0.5$, $\mathbb{L} = 100$ and $\Delta\wp = 0.01$ is shown in Figure 17. We conclude that we get closer to the exact solution as the fractional parameter increases.

Table 13. Exact and numerical solution for different values of $\mathfrak{B}$ when $\mathbb{L} = 100$, $\wp = 1$ and $\Delta\wp = 0.01$ for Example 5.4.

ε	$\mathfrak{B} = 0.3$	$\mathfrak{B} = 0.5$	$\mathfrak{B} = 0.7$	$\mathfrak{B} = 0.9$	Exact solution
0.0	0.00000	0.00000	0.00000	0.00000	0.00000
0.1	0.30647	0.30697	0.30878	0.30911	0.30902
0.2	0.58445	0.58470	0.58723	0.58796	0.58779
0.3	0.80504	0.80502	0.80812	0.80927	0.80902
0.4	0.94656	0.94624	0.94979	0.95138	0.95106
0.5	0.99512	0.99446	0.99834	1.00038	1.00000
0.6	0.94595	0.94490	0.94899	0.95149	0.95106
0.7	0.80390	0.80240	0.80653	0.80949	0.80902
0.8	0.58297	0.58096	0.58489	0.58821	0.58779
0.9	0.30512	0.30247	0.30577	0.30894	0.30902
1.0	0.00000	0.00000	0.00000	0.00000	0.00000

Table 14. Error norms L_∞ and L_2 for Example 5.4 when $\mathfrak{B} = 0.50$.

$\mathfrak{h} = \Delta\wp$	$\wp = 0.2$		$\wp = 0.4$		$\wp = 0.6$		$\wp = 0.8$	
	L_∞	L_2	L_∞	L_2	L_∞	L_2	L_∞	L_2
$\frac{1}{100}$	2.06027×10^{-4}	1.45760×10^{-4}	4.93176×10^{-4}	3.51835×10^{-4}	8.03525×10^{-4}	5.69530×10^{-4}	3.31259×10^{-3}	1.29496×10^{-3}
$\frac{1}{150}$	1.14290×10^{-4}	8.08707×10^{-5}	2.70994×10^{-4}	1.93319×10^{-4}	4.39697×10^{-4}	3.10886×10^{-4}	2.06247×10^{-3}	7.77378×10^{-4}
$\frac{1}{200}$	7.50698×10^{-5}	5.31225×10^{-5}	1.77016×10^{-4}	1.26263×10^{-4}	2.86791×10^{-4}	2.02305×10^{-4}	1.46990×10^{-3}	5.42864×10^{-4}
$\frac{1}{250}$	5.41229×10^{-5}	3.83025×10^{-5}	1.27161×10^{-4}	9.06862×10^{-5}	2.05925×10^{-4}	1.44956×10^{-4}	1.12725×10^{-3}	4.11152×10^{-4}
$\frac{1}{300}$	4.14017×10^{-5}	2.93012×10^{-5}	9.70154×10^{-5}	6.91779×10^{-5}	1.57118×10^{-4}	1.10388×10^{-4}	9.09107×10^{-4}	3.27633×10^{-4}
$\frac{1}{350}$	3.29960×10^{-5}	2.33530×10^{-5}	7.71636×10^{-5}	5.50141×10^{-5}	1.25004×10^{-4}	8.76740×10^{-5}	7.56510×10^{-4}	2.70346×10^{-4}

Table 15. Order of convergence for Example 5.4 when $\mathbb{L} = 50$ and $\mathfrak{B} = 0.50$.

$\Delta\wp$	L_∞	EOC	CPU time (s)
$\frac{1}{10}$	1.95329×10^{-2}	–	0.10937
$\frac{1}{20}$	6.93789×10^{-3}	1.49333	0.3125
$\frac{1}{40}$	2.48180×10^{-3}	1.48311	0.57812
$\frac{1}{80}$	8.90657×10^{-4}	1.47845	1.0251
$\frac{1}{160}$	3.30056×10^{-4}	1.43216	1.40625

The piece-wise spline solution for Example 5.4 at $\wp = 1$, $\mathbb{L} = 100$ and $\Delta\wp = 0.01$ is given as

$$\mathbb{S}(\varepsilon, 1) = \begin{cases} 216.111\cos\frac{\varepsilon}{2} - 216.111\cos\left(\frac{\varepsilon}{2}\right)^3 - 17966.1\sin\left(\frac{\varepsilon}{2}\right)^3 + \\ 13474.6\sin\varepsilon^2 + \sin\frac{\varepsilon}{2}(-53894.9 + 324.166\sin\varepsilon), & \text{if } \varepsilon \in [0, \frac{1}{100}], \\ -154.373\cos\frac{\varepsilon}{2} + 154.361\cos\left(\frac{\varepsilon}{2}\right)^3 + 6730.13\sin\left(\frac{\varepsilon}{2}\right)^3 + \\ \sin\frac{\varepsilon}{2}(20201.2 - 231.541\sin\varepsilon) - 5047.6\csc\frac{\varepsilon}{2}\sin\varepsilon^2, & \text{if } \varepsilon \in [\frac{1}{100}, \frac{2}{100}], \\ 277.673\cos\frac{\varepsilon}{2} - 277.627\cos\left(\frac{\varepsilon}{2}\right)^3 - 7665.16\sin\left(\frac{\varepsilon}{2}\right)^3 + \\ 5748.87\csc\frac{\varepsilon}{2}\sin\varepsilon^2 + \sin\frac{\varepsilon}{2}(-23001.9 + 416.441\sin\varepsilon), & \text{if } \varepsilon \in [\frac{2}{100}, \frac{3}{100}], \\ \quad\vdots \qquad\qquad \vdots \qquad\qquad \vdots & \\ 43405.8\cos\frac{\varepsilon}{2} - 39509.9\cos\left(\frac{\varepsilon}{2}\right)^3 - 39354.5\sin\left(\frac{\varepsilon}{2}\right)^3 + \\ 29515.9\csc\frac{\varepsilon}{2}\sin\varepsilon^2 + \sin\frac{\varepsilon}{2}(-161564. + 59264.9\sin\varepsilon), & \text{if } \varepsilon \in [\frac{49}{100}, \frac{50}{100}], \\ -44749.5\cos\frac{\varepsilon}{2} + 40582.5\cos\left(\frac{\varepsilon}{2}\right)^3 + 39214.4\sin\left(\frac{\varepsilon}{2}\right)^3 + \\ \sin\frac{\varepsilon}{2}(163273. - 60873.7\sin\varepsilon) - 29410.8\csc\frac{\varepsilon}{2}\sin\varepsilon^2, & \text{if } \varepsilon \in [\frac{50}{100}, \frac{51}{100}], \\ \quad\vdots \qquad\qquad \vdots \qquad\qquad \vdots & \\ -75843.\cos\frac{\varepsilon}{2} + 53651.7\cos\left(\frac{\varepsilon}{2}\right)^3 + 5820.33\sin\left(\frac{\varepsilon}{2}\right)^3 + \\ \sin\frac{\varepsilon}{2}(143024. - 80477.5\sin\varepsilon) - 4365.25\csc\frac{\varepsilon}{2}\sin\varepsilon^2, & \text{if } \varepsilon \in [\frac{97}{100}, \frac{98}{100}], \\ 68605.4\cos\frac{\varepsilon}{2} - 48138.5\cos\left(\frac{\varepsilon}{2}\right)^3 - 4474.63\sin\left(\frac{\varepsilon}{2}\right)^3 + \\ 3355.97\csc\frac{\varepsilon}{2}Sin\varepsilon^2 + \sin\frac{\varepsilon}{2}(-127789. + 72207.7\sin\varepsilon), & \text{if } \varepsilon \in [\frac{98}{100}, \frac{99}{100}], \\ -45152.4\cos\frac{\varepsilon}{2} + 31392.6\cos\left(\frac{\varepsilon}{2}\right)^3 + 2365.64\sin\left(\frac{\varepsilon}{2}\right)^3 + \\ \sin\frac{\varepsilon}{2}(82941. - 47088.9\sin\varepsilon) - 1774.23\csc\frac{\varepsilon}{2}\sin\varepsilon^2, & \text{if } \varepsilon \in [\frac{99}{100}, 1]. \end{cases} \tag{5.8}$$

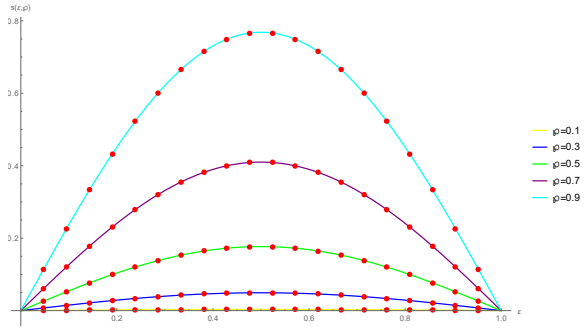

Figure 14. Graph of numerical and exact solutions when $\mathbb{L} = 100$, $\Delta\wp = 0.01$ and $\mathfrak{B} = 0.50$.

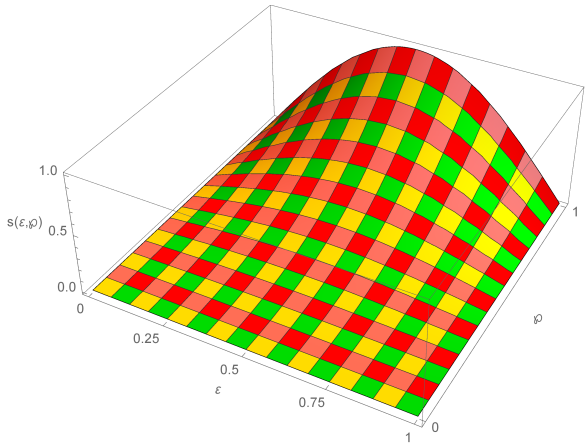

Figure 15. Three-dimensional view of exact solutions for Example 5.4 when $\mathbb{L} = 100$, $\Delta\wp = 0.01$ and $\mathfrak{B} = 0.50$.

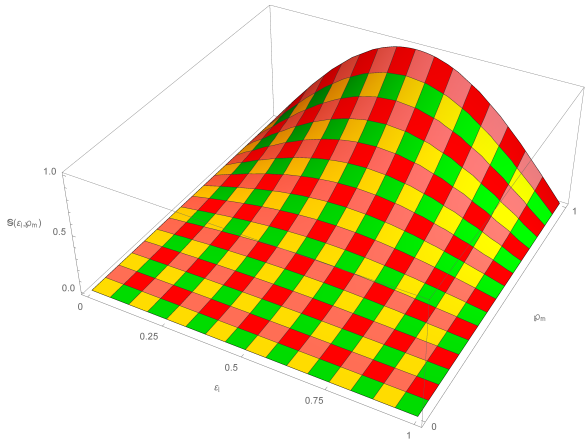

Figure 16. Three-dimensional view of numerical results for Example 5.4 when $\mathbb{L} = 100$, $\Delta\wp = 0.01$ and $\mathfrak{B} = 0.50$.

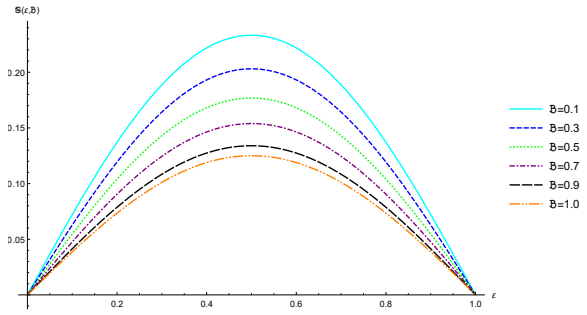

Figure 17. The behavior of different fractional order $\mathfrak{B}$ on approximate solutions for Example 5.4 corresponding to $\wp = 0.5$, $\mathbb{L} = 100$ and $\Delta\wp = 0.01$.

6. Conclusions

The authors summarize this work as follows:

- A computational method based on trigonometric cubic B-spline functions has been presented for the numerical simulation of nonlinear time fractional gas dynamics equation.
- The typical finite difference formulation has been used to discretize the Caputo time fractional derivative.
- The trigonometric B-spline functions have been used to interpolate the solution curve along the spatial direction.
- The theoretical results for stability and convergence analysis show that the proposed numerical scheme is conditionally stable.
- To check the efficiency and effectiveness of the presented scheme, the results of four numerical experiments, with known exact solutions, have been reported.
- The experimental order of convergence has shown to be $O(\Delta\wp)^{2-\mathfrak{B}}$ in temporal direction, while in spatial direction it is slightly less than our theoretical expectations.
- Unlike the usual finite difference approaches that only yield numerical solutions at pre-selected points of the spatial domain, the presented scheme can obtain numerical values of unknown function and its derivatives at non-grid points as well.
- The obtained results have been compared with exact solutions and the approximate results reported in the literature. The current method provides more accurate results as compared to the cubic B-spline collocation method, quadratic B-spline Galerkin method and differential transform method.
- The proposed numerical method is simple, straightforward to apply and efficiently approximates the solution curve. Hence, it can be confidently used to solve many similar nonlinear models whose exact solutions are not available.

Use of AI tools declaration

The authors declare they have not used Artificial Intelligence (AI) tools in the creation of this article.

Conflict of interest

The authors declare that they have no conflicts interests.

References

1. O. A. Arqub, B. Maayah, Modulation of reproducing kernel Hilbert space method for numerical solutions of Riccati and Bernoulli equations in the Atangana-Baleanu fractional sense, *Chaos Solitons Fract.*, **125** (2019), 163–170. https://doi.org/10.1016/j.chaos.2019.05.025
2. Z. Odibat, S. Momani, V. S. Erturk, Generalized differential transform method: Application to differential equations of fractional order, *Appl. Math. Comput.*, **197** (2008), 467–477. https://doi.org/10.1016/j.amc.2007.07.068
3. X. B. Yin, S. Kumar, D. Kumar, A modified homotopy analysis method for solution of fractional wave equations, *Adv. Mech. Eng.*, **7** (2015), 12. https://doi.org/10.1177/1687814015620330
4. X. X. Li, C. H. He, Homotopy perturbation method coupled with the enhanced perturbation method, *J. Low Freq. Noise Vib. Active Control*, **38** (2019), 1399–1403. https://doi.org/10.1177/1461348418800554
5. B. Ibis, The approximate solutions of fractional gas dynamics equations by means of fractional natural decomposition method, *New Trends Math. Sci.*, **5** (2017), 271–279. https://doi.org/10.20852/ntmsci.2017.238
6. S. Das, R. Kumar, Approximate analytical solutions of fractional gas dynamic equations, *Appl. Math. Comput.*, **217** (2011), 9905–9915. https://doi.org/10.1016/j.amc.2011.03.144
7. T. R. R. Rao, R. S. Balaji, Numerical solution of time fractional gas dynamics equation, *Int. J. Eng. Technol.*, **7** (2018), 610–612. https://doi.org/10.14419/ijet.v7i4.10.21294
8. K. S. Saad, E. H. Al-Shareef, M. S. Mohamed, X. J. Yang, Optimal q-homotopy analysis method for time-space fractional gas dynamics equation, *Eur. Phys. J. Plus*, **132** (2017), 1–11. https://doi.org/10.1140/epjp/i2017-11303-6
9. N. Iqbal, A. Akgül, R. Shah, A. Bariq, M. M. Al-Sawalha, A. Ali, On solutions of fractional-order gas dynamics equation by effective techniques, *J. Funct. Spaces*, **2022** (2022), 1–14. https://doi.org/10.1155/2022/3341754
10. G. Fairweather, D. Meade, A survey of spline collocation methods for the numerical solution of differential equations, In: *Mathematics for large scale computing*, Boca Raton: CRC Press, 1989.
11. B. Bialecki, G. Fairweather, A. Karageorghis, Matrix decomposition algorithms for modified spline collocation for Helmholtz problems, *SIAM J. Sci. Comput.*, **24** (2003), 1733–1753. https://doi.org/10.1137/S106482750139964X
12. B. Bialecki, G. Fairweather, Orthogonal spline collocation methods for partial differential equations, *J. Comput. Appl. Math.*, **128** (2001), 55–82. https://doi.org/10.1016/S0377-0427(00)00509-4
13. A. Esen, O. Tasbozan, Cubic B-spline collocation method for solving time fractional gas dynamics equation, *Tbilisi Math. J.*, **8** (2015), 221–231. https://doi.org/10.1515/tmj-2015-0024

14. A. Esen, O. Tasbozan, An approach to time fractional gas dynamics equation: Quadratic B-spline Galerkin method, *Appl. Math. Comput.*, **261** (2015), 330–336. https://doi.org/10.1016/j.amc.2015.03.126
15. G. Z. Wang, Q. Y. Chen, M. H. Zhou, NUAT B-spline curves, *Comput. Aided Geom. Des.*, **21** (2004), 193–205. https://doi.org/10.1016/j.cagd.2003.10.002
16. T. Nazir, M. Abbas, A. I. M. Ismail, A. A. Majid, A. Rashid, The numerical solution of advection-diffusion problems using new cubic trigonometric B-splines approach, *Appl. Math. Model.*, **40** (2016), 4586–4611. https://doi.org/10.1016/j.apm.2015.11.041
17. B. Ay, I. Dag, M. Z. Gorgulu, Trigonometric quadratic B-spline subdomain Galerkin algorithm for the Burgers' equation, *Open Phys.*, **13** (2015), 400–406. https://doi.org/10.1515/phys-2015-0059
18. M. Yaseen, M. Abbas, A. I. Ismail, T. Nazir, A cubic trigonometric B-spline collocation approach for the fractional sub-diffusion equations, *Appl. Math. Comput.*, **293** (2017), 311–319. https://doi.org/10.1016/j.amc.2016.08.028
19. M. Yaseen, M. Abbas, B. Ahmad, Numerical simulation of the nonlinear generalized time-fractional Klein-Gordon equation using cubic trigonometric B-spline functions, *Math. Methods Appl. Sci.*, **44** (2021), 901–916. https://doi.org/10.1002/mma.6798
20. M. Yaseen, M. Abbas, M. B. Riaz, A collocation method based on cubic trigonometric B-splines for the numerical simulation of the time-fractional diffusion equation, *Adv. Differ. Equ.*, **2021** (2021), 1–19. https://doi.org/10.1186/s13662-021-03360-6
21. M. Abbas, A. A. Majid, A. I. M. Ismail, A. Rashid, The application of cubic trigonometric B-spline to the numerical solution of the hyperbolic problems, *Appl. Math. Comput.*, **239** (2014), 74–88. https://doi.org/10.1016/j.amc.2014.04.031
22. S. G. Rubin, R. A. Graves, Viscous flow solutions with a cubic spline approximation, *Comput. Fluids*, **3** (1975), 1–36. https://doi.org/10.1016/0045-7930(75)90006-7
23. N. Khalid, M. Abbas, M. K. Iqbal, Non-polynomial quintic spline for solving fourth-order fractional boundary value problems involving product terms, *Appl. Math. Comput.*, **349** (2019), 393–407. https://doi.org/10.1016/j.amc.2018.12.066
24. M. Yaseen, M. Abbas, An efficient computational technique based on cubic trigonometric B-splines for time fractional Burgers' equation, *Int. J. Comput. Math.*, **97** (2020), 725–738. https://doi.org/10.1080/00207160.2019.1612053
25. W. K. Zahra, Trigonometric B-spline collocation method for solving PHI-four and Allen-Cahn equations, *Med. J. Math.*, **14** (2017), 1–19. https://doi.org/10.1007/s00009-017-0916-8

AIMS Press